AEDC-TN-59-11
ASTIA DOCUMENT NO.:
AD-306443

[redacted]

DOCUMENT NO. ______
This is copy number 1
of 40, which consists of
44 pages, series A.

(TITLE UNCLASSIFIED)

ALTITUDE PERFORMANCE EVALUATION OF TWO AFTERBURNER FUEL MANIFOLD CONFIGURATIONS IN AN IROQUOIS SERIES 2 TURBOJET ENGINE

By
T. R. Ward and James Neely
ETF, ARO, Inc.

April 1959

ARNOLD ENGINEERING DEVELOPMENT CENTER

AIR RESEARCH AND DEVELOPMENT COMMAND

US AF

[redacted]

AEDC-TN-59-11
ASTIA DOCUMENT NO.:
AD-306443

(Title Unclassified)

ALTITUDE PERFORMANCE EVALUATION OF TWO AFTERBURNER FUEL MANIFOLD CONFIGURATIONS IN AN IROQUOIS SERIES 2 TURBOJET ENGINE

By

T. R. Ward and James Neely

ETF, ARO, Inc.

April 1959

System - Canadian CF 105 (Arrow Interceptor)

Project 3066 - Task 30532
ARO Project No. 121841

Contract No. AF 40(600)-700 S/A 13(59-1)

CONTENTS

ILLUSTRATIONS

ABSTRACT

At the request of Headquarters, United States Air Force, an investigation was conducted to determine the relative performance of two afterburner fuel manifold configurations in an Orenda Engines Ltd. Iroquois series 2 turbojet engine. Performance data were recorded at a constant engine inlet temperature of 560° R and at a constant high pressure rotor speed of 7650 rpm for engine inlet pressures ranging from approximately 2 to 8 psia. The results indicate that the performance of the single entry manifold configuration was equal to or better than that of the triple entry manifold configuration at most of the conditions tested.

Limited compressor performance data were obtained at a Reynolds number index of 0.37 with exhaust nozzle areas ranging from 4.5 to 5.28 sq ft. Some overall engine performance results are also included.

NOMENCLATURE

A	Area, ft^2
a	Speed of sound at simulated flight altitude
C_d	Exhaust nozzle discharge coefficient
C_f	Flow coefficient
$C_{F_{j_{cn}}}$	Ratio of actual jet thrust to jet thrust produced by an ideal convergent nozzle expansion of gas at jet pipe conditions to test chamber condition
$C_{F_{j_{is}}}$	Ratio of actual jet thrust to jet thrust produced by isentropic expansion of gas at jet pipe conditions to test chamber conditions
F	Thrust, lb
F_{js}	Jet thrust obtained from scale force, lb
F_s	Scale force
f	Fuel-air ratio
F_r	Simulated flight inlet momentum, lb
g	Acceleration due to gravity, 32.14 ft/sec^2
GV	High pressure compressor inlet guide vane position, deg
H	Enthalpy, Btu/lb
h_L	Lower heating value of fuel, Btu/lb

M	Mach number
m	Mass rate of flow, lb-sec/ft
N_1	Rotational speed of low pressure compressor-turbine rotor, rpm
N_2	Rotational speed of high pressure compressor-turbine rotor, rpm
P	Total pressure, psfa, psia
p	Static pressure, psfa, psia
PLP	Power lever position, deg
R	Gas constant, 53.34 ft-lb/lb-°R
Re_I	Reynolds number index
RF	Thermocouple impact-recovery factor
SFC	Specific fuel consumption
T	Total temperature, °R
t	Static temperature, °R
V	Velocity, ft/sec
W	Weight rate of flow, lb/sec, lb/hr
γ	Ratio of specific heat at constant pressure to specific heat at constant volume.
δ	Ratio of absolute total pressure to absolute total pressure at sea-level static conditions of ARDC model atmosphere (2116 psfa)
ΔH	Change in enthalpy, Btu/lb
η	Efficiency
θ	Ratio of absolute total temperature to absolute total temperature at sea-level static conditions of ARDC model atmosphere (518.7°R)
ϕ	Ratio of absolute viscosity to absolute viscosity at sea-level static conditions of ARDC model atmosphere

SUBSCRIPTS

a	Air
ab	Afterburner
adj	Related to simulated flight conditions

b	Burner
bl	Station 4 overboard bleed
c	Compressor
cc	Combustion chamber
cn	Ideal convergent exhaust nozzle
e	Engine
eff	Effective
f	Fuel
g	Gas
hp	High pressure compressor
i	Indicated
is	Isentropic
j	Jet
lp	Low pressure compressor
m	Pressure loss due to heat addition
n	Net
s	Scale
t	Total
tp	Tailpipe
tu	Turbine
x	Effective duct outside diameter in labyrinth seal plane
00, 0, 1 2, 3, etc	Instrumentation station locations
1n	Venturi throat
10s	Exhaust nozzle static pressure
∞	Equivalent free-stream conditions

INTRODUCTION

At the request of Headquarters, United States Air Force, a testing program was conducted at the Engine Test Facility, Arnold Engineering Development Center (ETF-AEDC), to evaluate the altitude performance of the Iroquois turbojet engine manufactured by Orenda Engines Ltd. Malton, Ontario, Canada.

The two objectives of the portion of the test reported here were to determine compressor performance and to determine the relative merits of two afterburner fuel manifold configurations used on the Iroquois engine. All testing was accomplished on a single Iroquois turbojet engine (S/N AX-102) during the period September 5 through October 13, 1958.

Since the second objective was the more important, it is treated more thoroughly in this report, and the results were more thoroughly documented. Only limited data were obtained pertaining to the first objective, and only typical performance plots are presented. Some overall engine performance results are also included. A summary of the mechanical operating experiences accumulated during the testing is presented in Ref. 1.

APPARATUS

ENGINE

The Orenda Iroquois series 2 engine (Fig. 1 and Ref. 2) is a two-spool axial flow turbojet engine with a close coupled afterburner designed for supersonic flight. It has a mechanical limitation of Mach number 2.0 at 38,000-ft altitude at hot day conditions or Mach number 2.13 at 36,000-ft altitude at standard day conditions.

The low pressure compressor-turbine spool consists of a three stage compressor driven by a single turbine stage. The high pressure compressor-turbine is made up of a seven stage compressor driven by a two stage turbine. Estimated sea-level static military thrust of the engine without afterburning is 18,570 lb at a low pressure rotor speed of 5740 rpm and a high pressure rotor speed of 7930 rpm (Ref. 3).

Manuscript released by authors February 1959.

The engine combustion system is composed of an annular combustion chamber and a vaporizing fuel system with 32 equally spaced fuel injection pipes.

The Iroquois afterburner (Fig. 2) consists basically of a flame stabilizing system, a short perforated internal liner immediately downstream of the gutters, two fuel manifolds, a jet pipe with an external shroud on the downstream portion only, and a fully modulating petal-type converging exhaust nozzle. The flame stabilizing system has an inner and an outer ring gutter with a fuel manifold immediately upstream of each gutter. A second afterburner fuel manifold is located approximately 13 in. upstream of the downstream fuel manifolds and radially midway between them.

The two afterburner fuel manifold configurations tested were the single entry fuel manifold configuration and the triple entry fuel manifold configuration. In addition, some data were taken during operation with the downstream manifold only.

The single entry fuel manifold configuration consisted of a single entry upstream fuel manifold (Fig. 3a) and the downstream fuel manifold (Fig. 3c). The triple entry fuel manifold consisted of a triple entry heat-shielded upstream manifold (Fig. 3b) used with the downstream manifold (Fig. 3c).

The single entry upstream manifold (Fig. 3a) is an oval cross-sectional tube having orifices drilled in the upstream edge for fuel spraying and only a single fuel entry line located at approximately the 180° position. The triple entry upstream fuel manifold (Fig. 3b) is heat-shielded, has three fuel entry lines, and utilizes a round cross-sectional tube with orifices facing upstream for fuel injection. The downstream fuel manifold (Fig. 3c) consists of ten separately fed independent manifolds of round cross-sectional tubing with orifices located in both the downstream edge and upstream edge for fuel injection. The upstream and downstream manifolds were supplied from the same source and operated at the same pressures when used simultaneously.

Engine and afterburner fuel flows were manually controlled.

The position of the exhaust nozzle during the engine checkout and engine evaluation portions of testing was manually controlled. The position of the exhaust nozzle during afterburning was controlled automatically to maintain a constant ratio of compressor discharge pressure to turbine discharge pressure of 3.2.

The engine was equipped with inlet guide vanes upstream of the high pressure compressor rotor; their position was manually controlled to meet the needs of the test.

INSTALLATION

The engine and air measuring venturi were installed in the altitude test chamber (Fig. 4 and Ref. 4), and the engine was attached to the exit of the air measuring venturi by means of a flexible boot. The front of the venturi, which was supported from the thrust stand with the engine, was suspended inside the labyrinth seals, which were attached to the rear face of the plenum chamber bulkhead, thus giving a "free-floating" unit.

Air was supplied through the cooling air manifold to maintain an indicated test chamber air temperature less than 610° R.

INSTRUMENTATION

Aerodynamic pressures and temperatures were measured at the stations shown in Fig. 5 with instrumentation as shown in Fig. 6.

The multiple probe rakes at stations 2, 3, 4, 7, 9, and 9a were designed to measure conditions at the centers of equal areas. Pressures and temperatures were measured at station 9a until the station 9a rake was removed for the afterburner testing. Inlet plenum pressure was indicated from two static orifices. Test chamber ambient pressure was indicated by four static orifices in the test chamber.

Aerodynamic pressures were recorded by photographing manometer boards in which mercury, tetrobromoethane, and water were used as indicating fluids. Temperatures were indicated on millivolt recorders and converted to degrees by a digital computer. The temperatures were tabulated in the control room immediately after each data run, and some specific performance parameters were tabulated to permit immediate evaluation of the validity of the data run.

Scale force measurements were obtained by the flexure-pivot-type thrust stand reacting against a strain-gage load cell mounted in the test chamber. Rotor speeds were indicated on events-per-unit-time counters. Liquid flows were sensed by turbine-type flowmeters and indicated on events-per-unit-time counters. Flowmeter calibrations were made using JP-4 fuel.

The nozzle position was sensed by a potentiometer and indicated by a null balance potentiometer system.

Observation of the burning characteristics during afterburning operation was accomplished through a periscope mounted in the test chamber exhaust ducting. In addition, color motion pictures were made of the burning characteristics; a copy is on file in the ETF-AEDC.

Certain compressor blade stresses, engine vibrations, the exhaust nozzle area, and engine rotor speeds were recorded on oscillographs during periods when engine speed, afterburner fuel flow, and engine inlet conditions were being changed.

PROCEDURE

Air at the temperature and pressure desired was supplied to the engine inlet. Performance was related to the simulated flight conditions which were defined by the engine inlet conditions, Aircraft Industries Association (AIA) inlet recovery, and the ARDC model atmosphere by means of the choked nozzle technique (Ref. 5). The test chamber ambient pressure surrounding the engine was set as near the desired altitude ambient pressure as the plant capabilities would allow.

In those cases in which the test chamber ambient pressure could not be set at the proper level to simulate the desired altitude, the overall performance was related to the desired altitude by an adjustment to the thrust values if the exhaust nozzle was choked. This adjustment is the product of the difference in pressure and the effective nozzle area and may be expressed as the ratio of effective velocities obtained with the desired exhaust nozzle pressure ratio to that obtained with the actual exhaust nozzle pressure ratio (See Appendix A). The parameters using this thrust are noted with the subscript "adj".

Certain parameters have been standardized to sea-level-standard conditions by the use of δ and θ (as defined in the Nomenclature) and are referred to as generalized.

The theoretical overall performance of the engine equipped with a hypothetical convergent-divergent nozzle with a throat area equal to the exhaust nozzle area and an exit area equal to 12.4375 sq ft was to be calculated if the tailpipe pressure were high enough to operate on design or underexpanded at the altitude conditions simulated. Since this was never the case, the calculation was not accomplished.

The testing was accomplished in three parts - engine checkout, engine performance evaluation, and afterburner evaluation.

ENGINE CHECKOUT

The engine checkout portion of testing was performed to determine that the engine and installation were functioning properly. Operation at 8 psia inlet total pressure and 560°R inlet total temperature was

possible, but the engine could not be operated at 4 psia engine inlet total pressure because of compressor surge.

COMPRESSOR PERFORMANCE EVALUATION

The compressor performance portion of the testing was limited to only two high pressure compressor rotor speeds (6000 and 6500 rpm) at each of four set exhaust nozzle areas between 4.65 and 5.28 sq ft. Operation at higher high pressure rotor speeds was not possible because of compressor surge. During this portion of the test, engine inlet total pressure was 4.0 psia, and engine inlet total temperature was 415° R.

Data were also obtained to indicate the engine surge limit in the operating area where the afterburner investigation was to be made using zero, 1.17 percent, and 2.34 percent high pressure compressor discharge overboard bleed. (Normal Iroquois engine operation utilizes a high pressure compressor discharge bleed of approximately 2 percent to drive the fuel pumps.)

AFTERBURNER EVALUATION

The afterburner evaluation portion of the testing was accomplished at the simulated flight conditions shown in Fig. 7. The Iroquois series 2 operating envelope is based on data presented in the model specification (Ref. 3). For all afterburning testing, engine inlet total temperature was 560° R, high pressure compressor rotor speed was 7650 rpm, and high pressure compressor inlet guide vane position was 0 deg.

Data were first obtained by using the single entry upstream fuel manifold configuration; random data runs were also made with the upstream manifold out of service, during which time operation was with the downstream manifold only. The single entry upstream fuel manifold was then replaced with the triple entry upstream manifold, and similar data runs were made. At each inlet pressure, data were obtained between lean and rich blowout or the limiting nozzle area. A summary of the afterburner data runs is shown in Fig. 8.

Data obtained to determine afterburner stability and blowout limits consisted of measurements of afterburner fuel flow and turbine discharge total pressure. These values were recorded manually from control room observations, and a full steady-state data point was not taken.

Engine power is identified by high pressure compressor rotor speed. The engine was operated within the manufacturer's tolerances for AEDC operation of this engine (Ref. 6).

Fuel used throughout the testing conformed to Mil-F-5624C grade JP-4 with a lower heating value of approximately 18,600 Btu/lb. Oil used throughout the testing conformed to Mil-L-7808C.

The methods of calculation used in the reduction of the data are given in Appendix A.

The data obtained during the test are tabulated in Appendix B (under separate cover). An explanation of the identification code is given on the first page of the Appendix. Identification of the column headings is given in this report.

RESULTS AND DISCUSSION

COMPRESSOR PERFORMANCE EVALUATION

The results obtained from the compressor performance evaluation portion of the testing are decidedly inconclusive in respect to the exact level of performance over a wide range of engine rotor speeds and exhaust nozzle areas. At each exhaust nozzle area set, an engine surge occurred before a high pressure rotor speed of 7000 rpm could be reached.

The limitation thus placed on the range of operation was so restrictive that first one, and then two, overboard bleed ports 1.92 in. in diameter were opened to bleed high pressure compressor discharge air. Bleed flow rate through each port was approximately 1.17 percent of compressor airflow. An indication of the effectiveness of this overboard bleed is shown in Fig. 9. The high pressure rotor speed at which stall would occur with the 2.34-percent overboard bleed was 6900 rpm at the minimum area tested, which is a generalized rotor speed of 7714 rpm. Since the highest generalized high pressure rotor speed to be attained during afterburner evaluation was 7363 rpm (7650 rpm at 560°R), this margin was felt to be safe.

AFTERBURNER EVALUATION

The afterburner fuel manifold flow characteristics are shown in Fig. 10. Ideally the relationship of flow rate to pressure drop of an incompressible fluid through an orifice should have a slope of 0.5 on a logarithmic plot. This was the case for all manifold configurations at the high flow rate end of the curves; however, as the flow rate was reduced, first the single entry configuration and then the triple entry configurations began to deviate. The downstream manifold did not

display any deviation from the straight line above a flow rate of approximately 4000 lb/hr and was quite close down to approximately 3000 lb/hr.

Since the gage used to indicate the upstream manifold pressure was connected to the fuel line which fed the manifold, rather than the manifold itself, there was some change in indicated pressure drop when the triple entry upstream manifold was installed. When this difference is taken into consideration and the change of the effective flow area of the systems is determined at approximately 6000 lb/hr, the single entry upstream manifold suffered a loss of approximately 24-percent effective area, and the triple entry upstream manifold lost approximately 6 percent of the effective area.

The afterburner stability limits shown in Fig. 11 are composed of burner blowout (bottom and left) and the limiting maximum exhaust nozzle area of 6.94 sq ft (top). The afterburner was considered to be out when burning became so negligible as to produce no effective heat release although localized burning continued at the lowest afterburning fuel flows that could be obtained; effective burning then began with an increase in afterburner fuel flow.

The turbine discharge pressures and afterburner fuel flows at which the single entry and the triple entry manifold configurations would operate are essentially the same at the low ends, within the accuracy with which the limits could be determined. However, combustion could be sustained at lower afterburner fuel flows in the higher turbine discharge pressure region with the single entry manifold configuration than with the triple entry manifold configurations. In fact, the single entry manifold configuration lean blowout line is very similar to that obtained during operation with the downstream manifold only. This is caused by the vaporization in the single entry upstream manifold at low afterburner flows, which causes a shift of larger percentages of the flow to the downstream manifold.

Afterburner combustion efficiencies obtained during the test are shown in Fig. 12. At the low values of afterburner fuel-air ratio, operation on the downstream manifold consistently displayed higher combustion efficiencies than with the configurations using the upstream manifolds, because of the better stability of the flame obtained with the fuel impingement on the flameholders. The apparent afterburner combustion efficiencies obtained with the single entry manifold configuration were generally higher than those obtained with the triple entry manifold configuration in the low and high afterburner fuel-air ratio ranges; the triple entry manifold configuration generally gave indications of efficiencies which were higher in the mid-range. It should be pointed out, however, that the indicated difference in combustion efficiency between the single entry and triple entry manifold configurations is generally within the scatter of the data values at all but the low afterburner fuel-air ratios.

OVERALL ENGINE PERFORMANCE

The engine pumping characteristics and engine generalized airflow vs generalized low pressure compressor rotor speed (Figs. 13 and 14) typify the engine performance results obtained. Generalized adjusted net thrust and generalized specific fuel consumption for nonafterburning operation at a constant high pressure rotor speed of 7650 rpm and at a constant Mach number of 1.47 over an altitude range from 43,000 to 63,400 ft are shown in Fig 15. The change in average generalized adjusted net thrust is shown to decrease only 1.6 percent from 43,000 ft to 63,400 ft. The average generalized specific fuel consumption over that range increases 3.8 percent.

The generalized specific fuel consumption vs generalized adjusted net thrust for afterburner operation is shown in Fig. 16. The trend in afterburner combustion efficiency (Fig. 12) at the higher pressure levels is also shown here; namely, the performance of the single entry and triple entry manifold configurations is generally the same in the mid range and the single entry manifold configuration indicates higher values of afterburner combustion efficiency and lower values of generalized specific fuel consumption at the low end. At the lower pressures, the smaller operating range and fewer data points do not permit the establishment of relationships with the same dependability as at the high pressure levels.

SUMMARY OF RESULTS

The results of the performance evaluation of an Iroquois AX-102 turbojet engine may be summarized as follows:

1. The overall performance with the single entry manifold configuration is equal to or better than that of the triple entry manifold configuration over most of the range tested.

2. The rate of afterburner fuel vaporization in the triple entry upstream manifold was much less than in the single entry upstream manifold in the lower afterburner fuel flow region; however, this vaporization in the single entry upstream manifold resulted in an extension of the operating range of the afterburner in the low afterburner fuel flow region.

3. Afterburner lean blowout during this test was somewhat of an elusive parameter since at many conditions spot burning continued although the effective heat release approached zero at the minimum fuel flow possible.

4. A severe surge problem existed during attempts to operate the engine at generalized rotor speeds as low as 7700 rpm.

5. The operational range of the high pressure compressor was improved by bleeding overboard up to 2.34 percent of the compressor airflow at the high pressure compressor discharge.

REFERENCES

1. Mayfield, Rupert C., "Mechanical Operating Experience With An Iroquois Turbojet Engine In An Altitude Test Chamber." AEDC-TN-58-101, January 1959. (Confidential)

2. Orenda Engines Limited, "Mechanical Description of the Iroquois Series 2." B4-58, March 1958. (Confidential)

3. Orenda Engines Limited, "Iroquois 2 Engine Preliminary Model Specification." EMS-8 Issue 2. (Confidential)

4. Test Facilities Handbook, (2nd Edition). "Engine Test Facility, Vol. 2." Arnold Engineering Development Center, January 1959.

5. Povolny, John, "Use of Choked Nozzle Technique and Exhaust Jet Diffuser for Extending Operable Range of Jet-Engine Research Facilities." NACA-RM E52E12, July 1952.

6. Britnell, Walter, "Operating Procedure for AEDC Testing of Iroquois Engine AX-102." July 8, 1958.

APPENDIX A

METHODS OF CALCULATION

TEMPERATURE

Total temperatures at stations 2, 3, 4, 7, and 9a were obtained by applying a recovery factor to the indicated temperature measurements in the calculation

$$T = \frac{T_i}{\left(\frac{p}{P}\right)^{\frac{\gamma-1}{\gamma}} + RF\left[1 - \left(\frac{p}{P}\right)^{\frac{\gamma-1}{\gamma}}\right]}$$

where RF = 0.85 (stations 2, 3, and 4)
and RF = 0.95 (stations 7 and 9a)

AIRFLOW

Airflow at stations 1n and 2 was calculated from the equation

$$W_a = \frac{pA\sqrt{\frac{2\gamma g}{\gamma-1}\left[1-\left(\frac{p}{P}\right)^{\frac{\gamma-1}{\gamma}}\right]}}{\sqrt{RT}\left(\frac{p}{P}\right)^{\frac{\gamma-1}{\gamma}}}$$

When the venturi was choked, airflow at station 1n was calculated from the expression

$$W_a = \frac{PA}{\sqrt{T}}\sqrt{\frac{\gamma g}{R}}\left(\frac{2}{\gamma+1}\right)^{\frac{\gamma+1}{2(\gamma-1)}}$$

Gas flow at stations 5 and 6a was determined by

$$W_{g_5} = W_{g_{6a}} = W_{a_{1n}} + W_{f_e} - 0.02\,W_{a_{1n}} - W_{a_{bl}}$$

where $0.02\,W_{a_{1n}}$ represents the manufacturer's approximation of the amount of cooling airflow extracted at station 4 and returned to the cycle at station 6. $W_{a_{bl}}$ in the above equation represents the overboard bleed air extracted at station 4. Overboard bleed air was calculated, using a port flow coefficient of 0.65, to be as follows:

Tests 02-10-1100 through 07-20-1100---0
Tests 08-20-1101----------0.0117 $W_{a_{1n}}$

Test 09-20-1102 through 17-30-1202---0.0234 Wa_{1n}

Gas flow at stations 6 and 7 was determined by

$$W_{g_6} = W_{g_7} = W_{a_{1n}} + W_{f_e} - W_{a_{bl}}$$

Gas flow at station 9 was determined by

$$W_{g_9} = W_{a_{1n}} + W_{f_e} + W_{f_{ab}} - W_{a_{bl}}$$

RATIO OF SPECIFIC HEATS

The ratio of specific heats, γ, was assumed to be 1.4 at stations 1 and 2. At the remaining engine stations, 3, 4, 5, 6, 7, 8, and 9, the variation due to gas temperature and composition was considered.

EQUIVALENT FLIGHT CONDITIONS

The free-stream total pressure was obtained by using the standard ram recovery proposed by AIA as in the expression

$$P_\infty = \frac{P_2}{1.0 - 0.1\,(M_\infty - 1.0)^{1.5}} \qquad \text{for } M_\infty \geq 1.0$$

and

$$P_\infty = P_2 \qquad \text{for } M_\infty < 1.0$$

Equivalent ambient temperature was calculated by the expression

$$t_\infty = \frac{T_2}{\left(\frac{P_\infty}{p_\infty}\right)^{\frac{\gamma-1}{\gamma}}}$$

Flight velocity was calculated by the expression

$$V_\infty = \sqrt{\frac{2\,\gamma\,g\,R\,t_\infty}{\gamma - 1}\left[\left(\frac{p_\infty}{P_\infty}\right)^{\frac{\gamma-1}{\gamma}} - 1\right]}$$

JET NOZZLE INLET TEMPERATURE

The jet nozzle inlet temperature for afterburner operation with the jet nozzle choked was obtained from the expression

$$T_{10} = \frac{2\gamma g}{R(\gamma + 1)} \left[\frac{P_9 \left(\frac{2}{\gamma + 1} \right)^{\frac{1}{\gamma - 1}}}{W_{g_9}} A_{10\,eff} \right]^2$$

For non-afterburner operation T_{10} was assumed equal to T_7.

EFFECTIVE NOZZLE AREA

Non-Afterburning

The effective nozzle area during non-afterburning operation was obtained from the following expressions

Nozzle Choked

$$A_{10_{eff}} = \frac{\sqrt{\frac{1}{\gamma} \left(\frac{2}{\gamma + 1} \right)}}{P_{10_s}} W_{g_7} \sqrt{\frac{R T_7}{g}}$$

Nozzle Unchoked

$$A_{10_{eff}} = \frac{\left(P_{10_s} / P_9 \right)^{\frac{\gamma - 1}{\gamma}}}{\sqrt{\frac{2\gamma}{\gamma - 1} \left[1 - \left(\frac{P_{10_s}}{P_9} \right)^{\frac{\gamma - 1}{\gamma}} \right]}} \left[\frac{W_{g_7}}{P_{10_s}} \sqrt{\frac{R T_7}{g}} \right]$$

Afterburning

The effective nozzle area during afterburning operation was obtained from the following equation

$$A_{10_{eff}} = C_d A_{10_i}$$

The exhaust nozzle coefficients (C_d) that were used are shown in Fig. 17.

FUEL-AIR RATIO

Engine fuel-air ratio was defined as

$$f_e = \frac{W_{f_e}}{W_{a_5}}$$

Afterburner fuel-air ratio was defined by the expression

$$f_{ab} = \frac{\left[(1 - \eta_b)\, W_{f_e} + W_{f_{ab}}\right]}{W_{a_9} - \eta_b\, (W_{f_e})\, 14.62}$$

where 14.62 was assumed equal to stoichiometric air-fuel ratio for the fuel used.

Total fuel-air ratio was obtained by the expression

$$f_t = \frac{W_{f_e} + W_{f_{ab}}}{W_{a_9}}$$

THRUST

Scale Thrust

Scale jet thrust at the desired flight condition was calculated from the equation

$$F_{j_{s_{adj}}}\left[F_s + M_{a_1} V_1 + A_{1x}\,(p_1 - p_0)\right]\left\{\frac{\left[\sqrt{2(\gamma_9 + 1)} - \left(\frac{p_\infty}{P_9}\right)\left(\frac{\gamma_9 + 1}{2}\right)^{\frac{\gamma_9 + 1}{2(\gamma_9 - 1)}}\right]}{\left[\sqrt{2(\gamma_9 + 1)} - \left(\frac{p_0}{P_9}\right)\left(\frac{\gamma_9 + 1}{2}\right)^{\frac{\gamma_9 + 1}{2(\gamma_9 - 1)}}\right]}\right\}$$

Net Thrust

Net thrust was then determined by

$$F_{n_{s_{adj}}} = F_{j_{s_{adj}}} - M_{a_1} V_\infty$$

Calculated Thrust

Ideal thrust for a converging nozzle was calculated from

$$F_{j_{cn}} = W_{g_9} \sqrt{\frac{R T_9}{g}} \left[\sqrt{\frac{2(\gamma+1)}{\gamma}} - \frac{\frac{P_0}{P_9}}{\sqrt{\gamma} \left(\frac{2}{\gamma+1}\right)^{\frac{\gamma+1}{2(\gamma-1)}}} \right]$$

Ideal thrust resulting from isentropic expansion to test chamber pressure was determined from the expression

$$F_{j_{is}} = W_{g_9} \sqrt{\frac{R T_9}{g}} \sqrt{\frac{2\gamma}{\gamma-1} \left[1 - \left(\frac{P_0}{P_9}\right)^{\frac{\gamma-1}{\gamma}} \right]}$$

Thrust Coefficient

The convergent nozzle thrust coefficient was defined as

$$C_{F_{j_{cn}}} = \frac{F_{j_s}}{F_{j_{cn}}}$$

and the isentropic thrust coefficient was defined as

$$C_{F_{j_{is}}} = \frac{F_{j_s}}{F_{j_{is}}}$$

COMBUSTION EFFICIENCY

The combustion efficiency in the main engine combustion chamber was determined from the following equation

$$\eta_b = \frac{W_{g_5} H_{g_5} - W_{a_5} H_{a_4} - 59.62 W_{f_e}}{h_L (W_{f_e})}$$

where the quantity 59.62 Btu/lb fuel accounts for the difference between the enthalpy of carbon dioxide and water vapor formed during combustion and the enthalpy of the oxygen removed from the air by their formation in the temperature range from 400°R (base of enthalpy equations) to 540°R (base temperature of determination of h_L).

The combustion efficiency of the afterburner was calculated from

$$\eta_{ab} = \frac{W_{g_9} H_{g_9} - W_{g_7} H_{g_7} - 59.62 [(1-\eta_b) W_{f_e} + W_{f_{ab}}]}{h_L [(1-\eta_b) W_{f_e} + W_{f_{ab}}]}$$

COMPRESSOR EFFICIENCY

The overall compressor efficiency was defined as

$$\eta_c = \frac{H_{a_{4_{is}}} - H_{a_2}}{H_{a_4} - H_{a_2}}$$

where $H_{a_{4_{is}}}$ is the theoretical enthalpy that would be obtained at station 4 if isentropic compression had been experienced.

The compressor efficiency of the low pressure compressor was obtained from

$$\eta_{c_{lp}} = \frac{H_{a_{3_{is}}} - H_{a_2}}{H_{a_3} - H_{a_2}}$$

The high pressure compressor efficiency was calculated from

$$\eta_{c_{hp}} = \frac{H_{a_{4_{is}}} - H_{a_3}}{H_{a_4} - H_{a_3}}$$

TURBINE EFFICIENCY

The turbine efficiency was defined as

$$\eta_{tu} = \frac{\left[1 - \left(\frac{T_7}{T_5}\right)\right]}{\left[1 - \left(\frac{P_7}{P_5}\right)^{\frac{\gamma_{tu} - 1}{\gamma_{tu}}}\right]}$$

where γ_{tu} was defined as being

$$\gamma_{tu} = \frac{\frac{(H_{g_5} - H_{g_2})}{(T_5 - T_7)}}{\frac{(H_{g_5} - H_{g_2})}{(T_5 - T_7)} - \frac{R}{778.3}}$$

TAILPIPE EFFICIENCY

The tailpipe efficiency was defined as

$$\eta_{tp} = \frac{\left(\frac{P_{8a}}{P_7}\right)^{\frac{\gamma_7 - 1}{\gamma_7}} - 1}{\frac{T_7 - t_7}{t_7}}$$

SPECIFIC FUEL COMSUMPTION

The specific fuel consumption was obtained from the following expressions

$$S\ F\ C = \frac{W_{f_e} + W_{f_{ab}}}{F_{n_{s_{adj}}}}$$

REYNOLDS NUMBER INDEX

The Reynold number index was calculated from the equation

$$Re_I = \frac{\delta_2}{\phi_2 \sqrt{\theta_2}} = \frac{\delta_2 (T_2 + 216)}{735\ \theta_2^2}$$

TURBINE INLET PRESSURE

The turbine inlet pressure was obtained from the expression

$$P_5 = P_4 \left[1 - 16.584 \left(\frac{W_{a_4} \sqrt{T_4}}{A_4\ P_4}\right)^2\right]$$

which was obtained from the engine manufacturer.

TURBINE INLET TEMPERATURE

The turbine inlet temperature was calculated by the iteration process from the following equation

$$H_{g_5} = \frac{0.2318\ T_5 + 0.052 \times 10^{-4} T_5^2 + 0.2388 \times 10^{-8} T_5^3 - 93.705}{1 + f_e}$$

$$+ f_e \left[0.2655\ T_5 + 1.8632 \times 10^{-4}\ T_5^2 - 2.2117 \times 10^{-8}\ T_5^3 - 134.60\right]$$

when T_5 is equal or less than 1700° R.

When T_5 is greater than 1700° R the following equation was used

$$H_{g_5} = \frac{0.2214\ T_5 + 0.176 \times 10^{-4}\ T_5^2 - 0.1258 \times 10^{-8}\ T_5^3 - 93.705}{1 + f_e}$$

$$+ \frac{f_e\ [0.3397\ T_5 + 1.359 \times 10^{-4}\ T_5^2 - 0.9861 \times 10^{-8}\ T_5^3 \quad 176.15]}{}$$

where

$$H_{g_5} = H_{g_7} + \frac{W_{a_2}}{W_{g_7}} (H_{a_3} - H_{a_2}) + \frac{W_{a_3}}{W_{g_5}} (H_{a_4} - H_{a_3})$$

PRESSURE LOSS DUE TO HEAT ADDITION

The tailpipe pressure loss due to heat addition was determined from the expression

$$\left[\frac{P_9}{P_8}\right]_m = \left(\frac{1 + \gamma_8 M_{8_a}^2}{1 + \gamma_9 M_9^2}\right) \left[\frac{\left(1 + \frac{\gamma_9 - 1}{2} M_9^2\right)^{\frac{\gamma_9}{\gamma_9 - 1}}}{\left(1 + \frac{\gamma_8 - 1}{2} M_{8_a}^2\right)^{\frac{\gamma_8}{\gamma_8 - 1}}}\right]$$

COMBUSTION CHAMBER VELOCITY

The combustion chamber velocity was calculated from the expression

$$V_{cc} = \frac{M_{cc} \sqrt{\gamma_9 R T_4}}{\sqrt{1 + \frac{\gamma - 1}{2} M_{cc}^2}}$$

and M_{cc} was determined from the equation

$$\frac{W_{a_5} \sqrt{T_4}}{P_4 A_{cc}} = \frac{\sqrt{\frac{\gamma_g}{R}}\ M_{cc}}{\left(1 + \frac{\gamma - 1}{2} M_{cc}^2\right)^{\frac{\gamma + 1}{2(\gamma - 1)}}}$$

where A_{cc} = 7.674 ft sq.

FLOW COEFFICIENT

The flow coefficients were determined by the expression

$$C_f = \frac{W_g \sqrt{T}}{AP \sqrt{\frac{2\gamma g}{R(\gamma-1)} \left[\left(\frac{p}{P}\right)^{\frac{2}{\gamma}} - \left(\frac{p}{P}\right)^{\frac{\gamma+1}{\gamma}} \right]}}$$

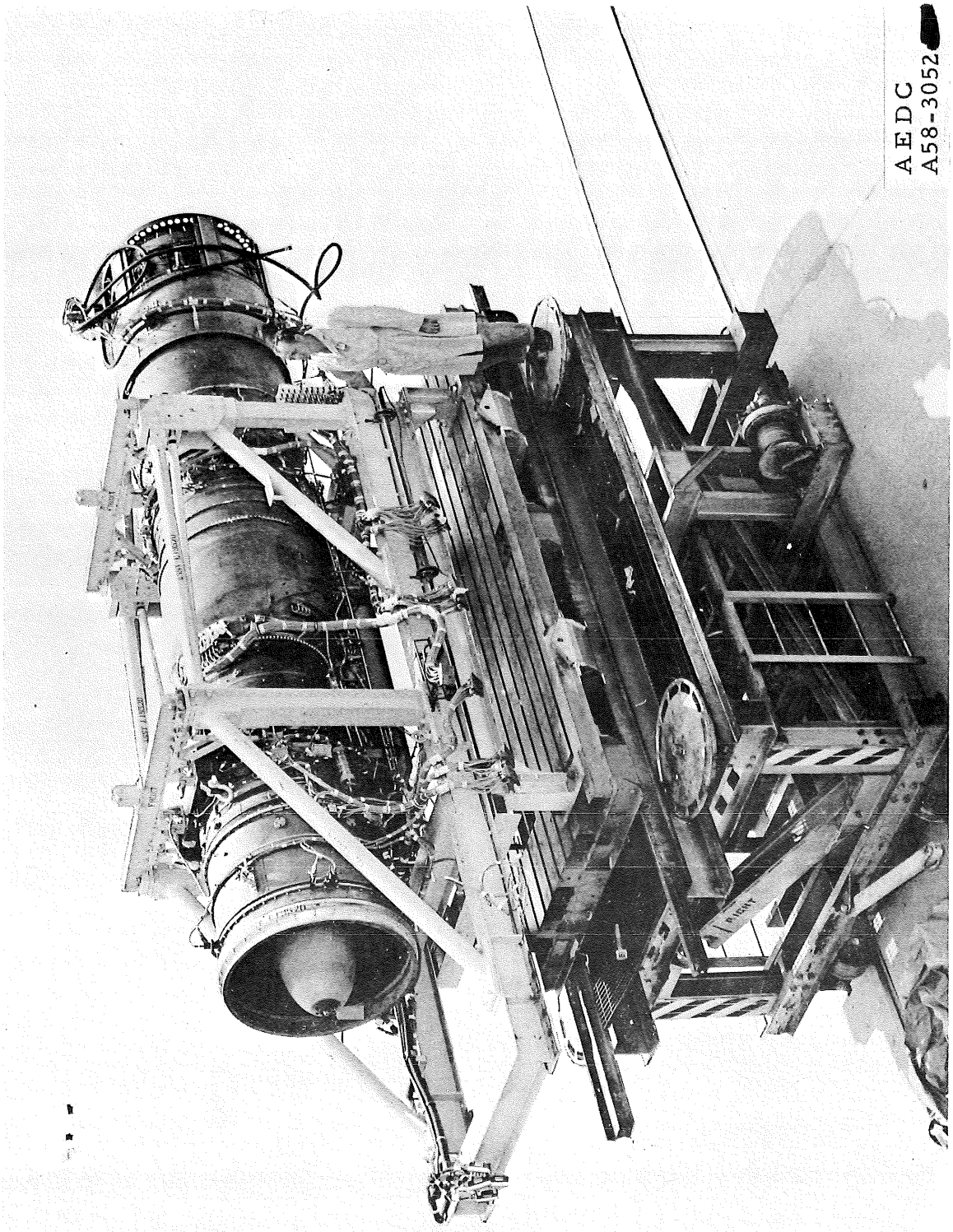

Fig. 1 Iroquois AX-102 Engine Prior to Installation in Test Chamber

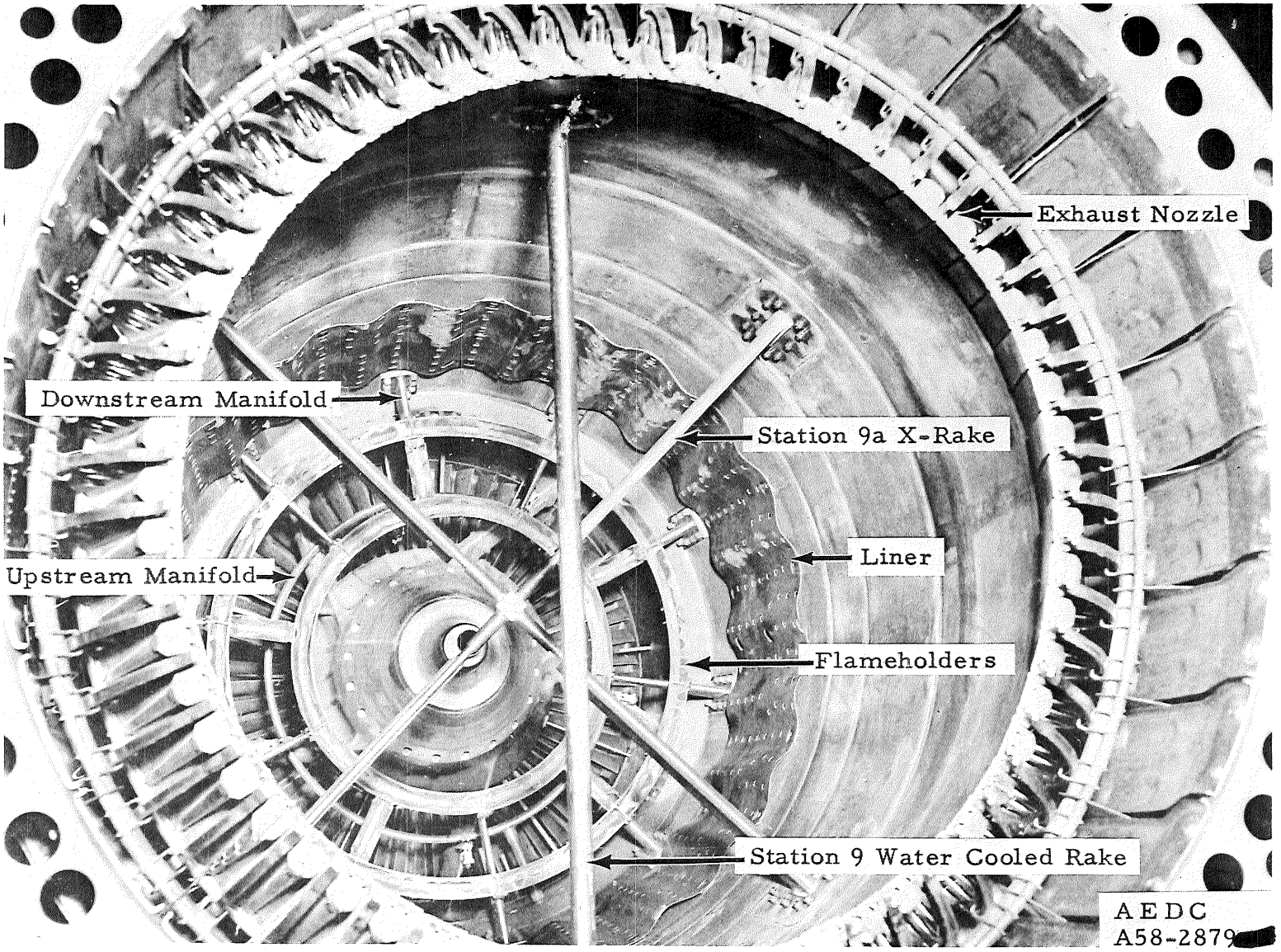

Fig. 2 Internal View of Iroquois Afterburner

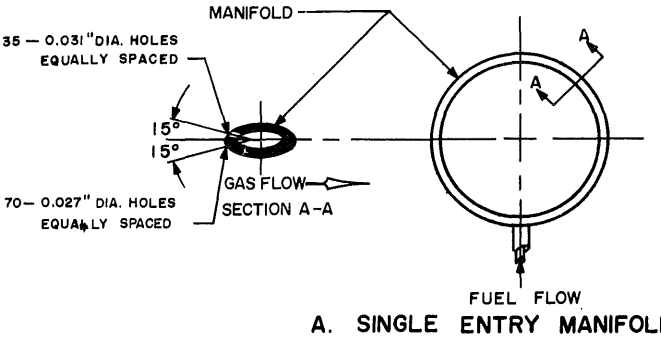

A. SINGLE ENTRY MANIFOLD

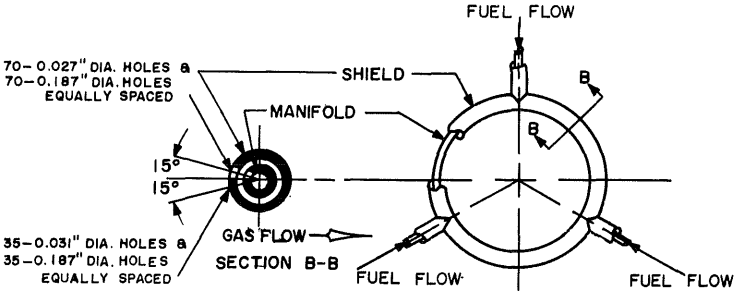

B. TRIPLE ENTRY MANIFOLD

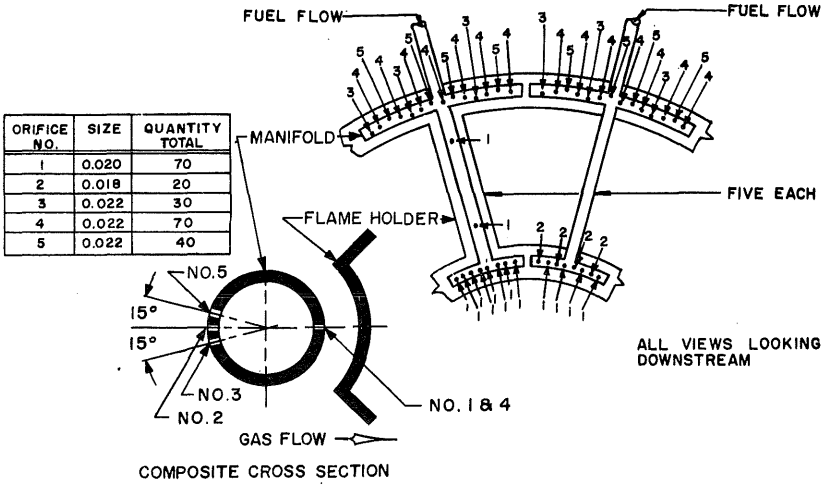

ORIFICE NO.	SIZE	QUANTITY TOTAL
1	0.020	70
2	0.018	20
3	0.022	30
4	0.022	70
5	0.022	40

COMPOSITE CROSS SECTION

C. DOWNSTREAM MANIFOLD

Fig. 3 Afterburner Fuel Manifolds

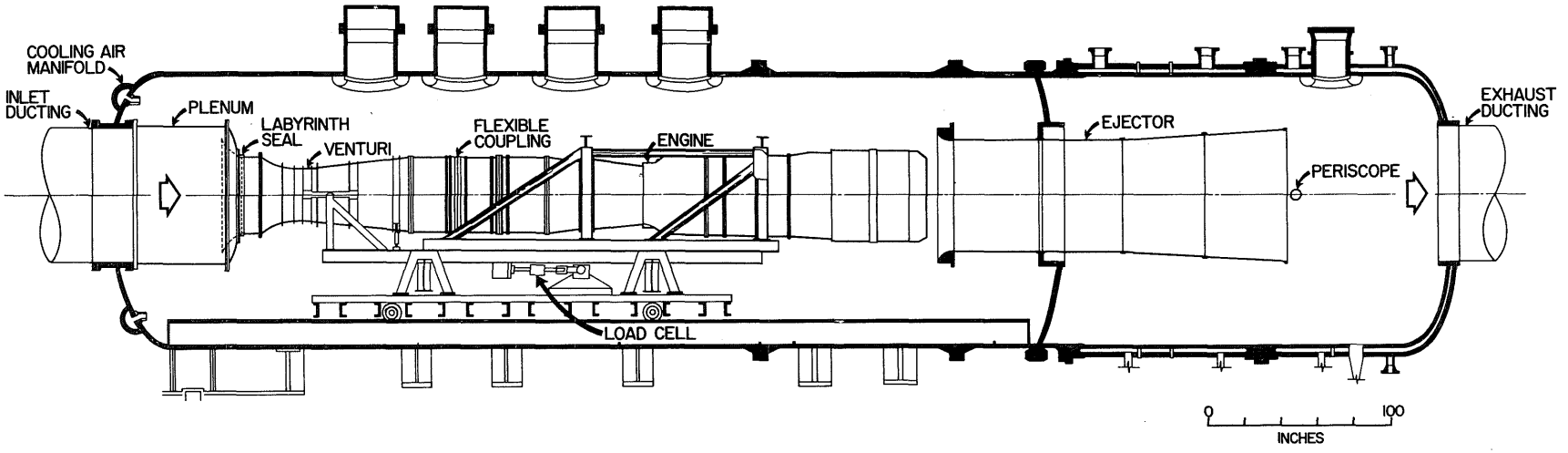

Fig. 4 Installation of Iroquois in Altitude Test Chamber

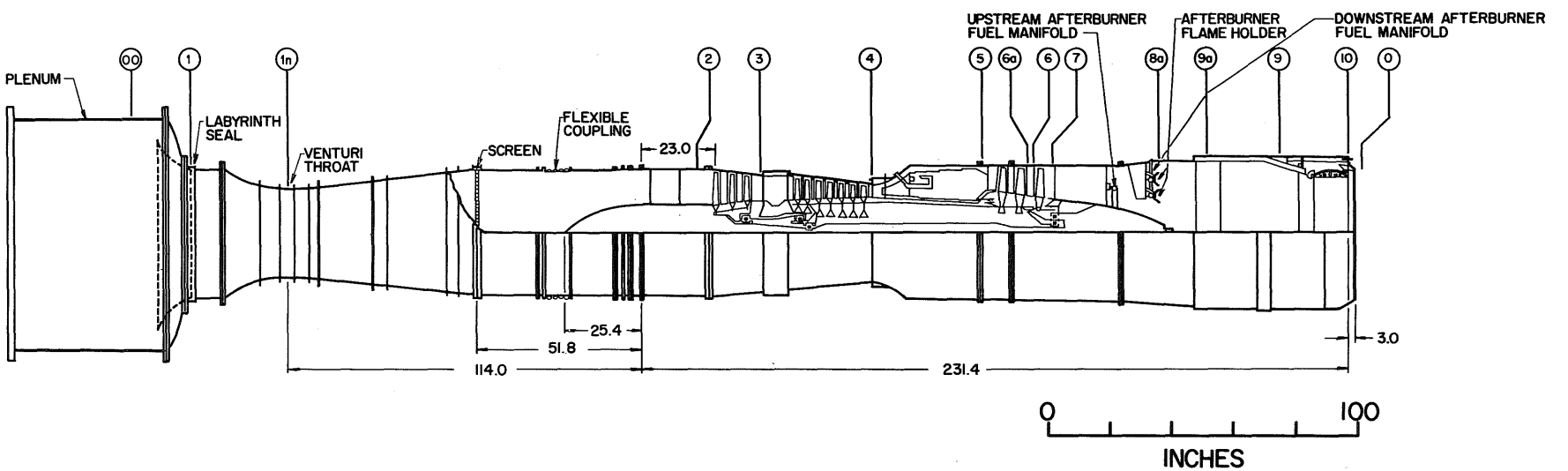

Fig. 5 Test Article Station Locations

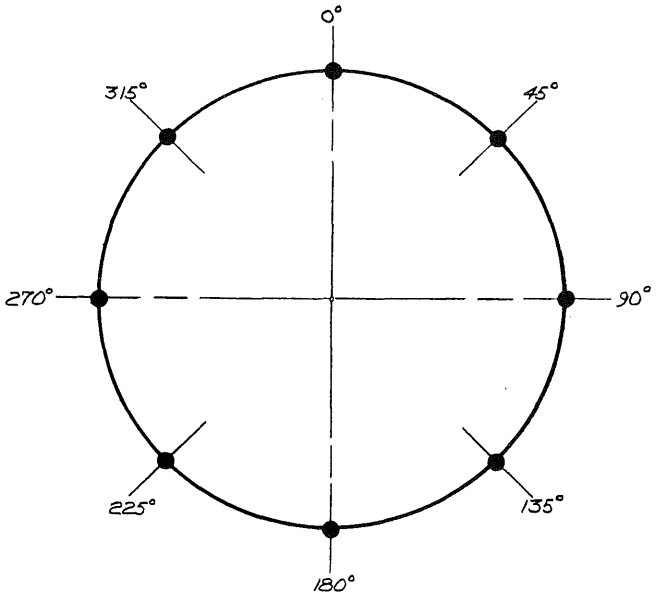

a. STATION 1n, VENTURI THROAT, 137 IN. UPSTREAM OF COMPRESSOR FRONT FACE

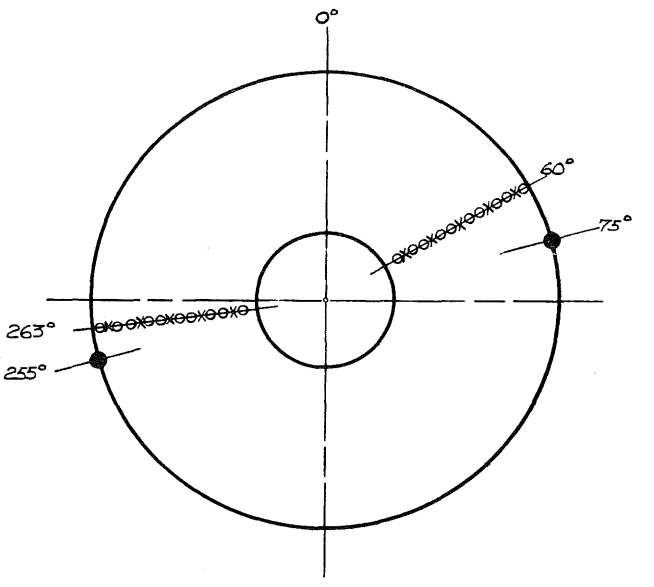

b. STATION 2, COMPRESSOR INLET, 5.25 IN UPSTREAM OF COMPRESSOR FRONT FACE

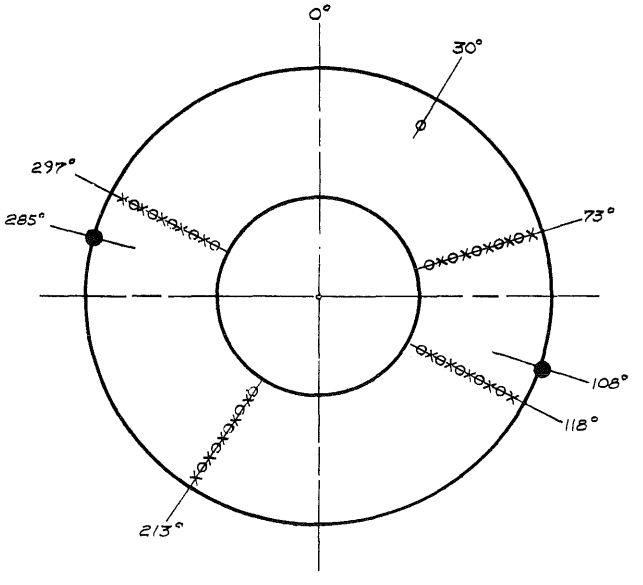

c. STATION 3, LOW PRESSURE COMPRESSOR DISCHARGE 1.38 IN. DOWNSTREAM OF STATOR EXIT

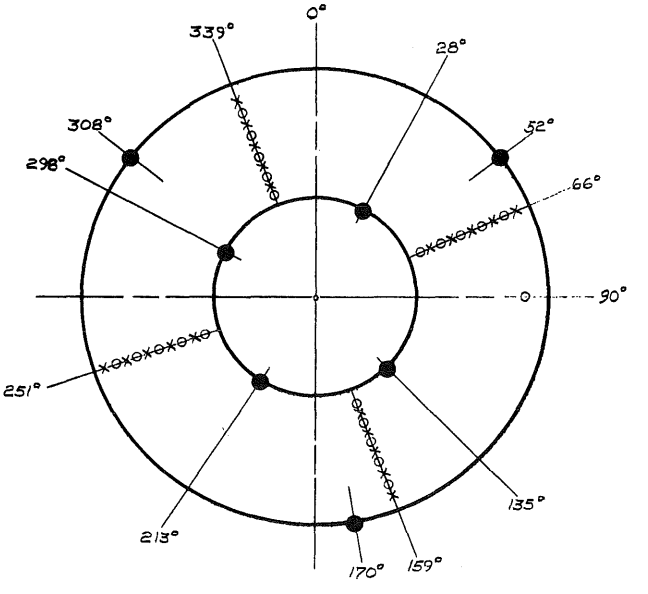

d. STATION 4, HIGH PRESSURE COMPRESSOR DISCHARGE 0.65 IN. DOWNSTREAM OF STATOR EXIT

o TOTAL PRESSURE
● STATIC PRESSURE
X THERMOCOUPLE

Fig. 6 Instrumentation Location Details (looking upstream)

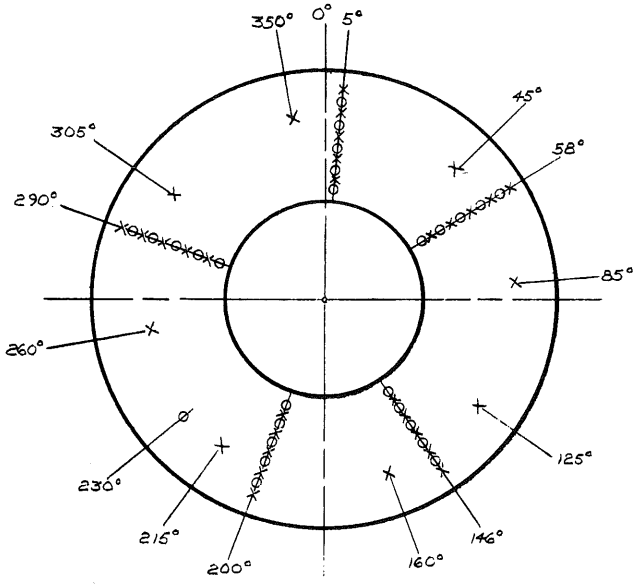

e. STATION 7, TURBINE DISCHARGE (SINGLE POINT THERMOCOUPLES ELECTRICALLY AVERAGED) 0.96 IN. DOWNSTREAM OF TURBINE DISCHARGE TRAILING EDGE AT MEAN CHORD

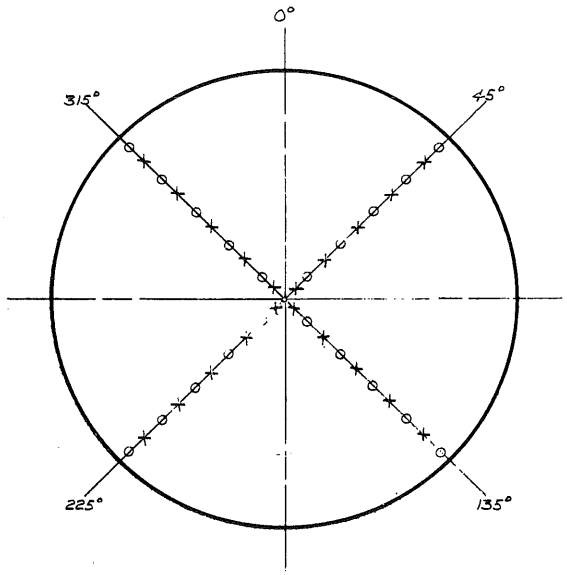

f. STATION 9a, AFTERBURNER, 38 IN. DOWNSTREAM OF AFTERBURNER FRONT FLANGE

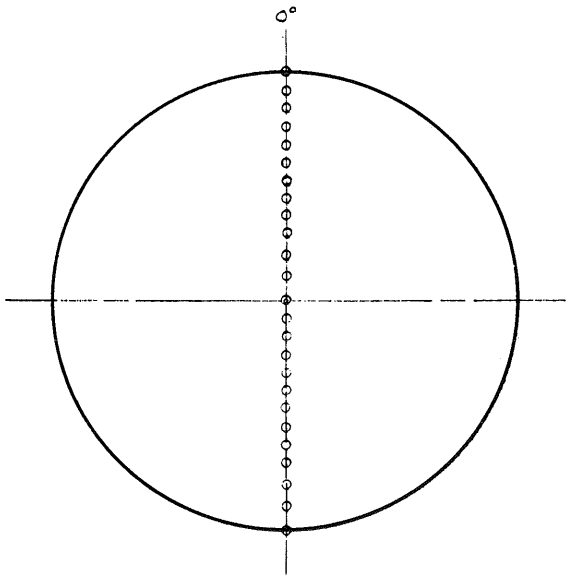

g. STATION 9, EXHAUST NOZZLE INLET 55.4 IN. DOWNSTREAM OF AFTERBURNER FRONT FLANGE

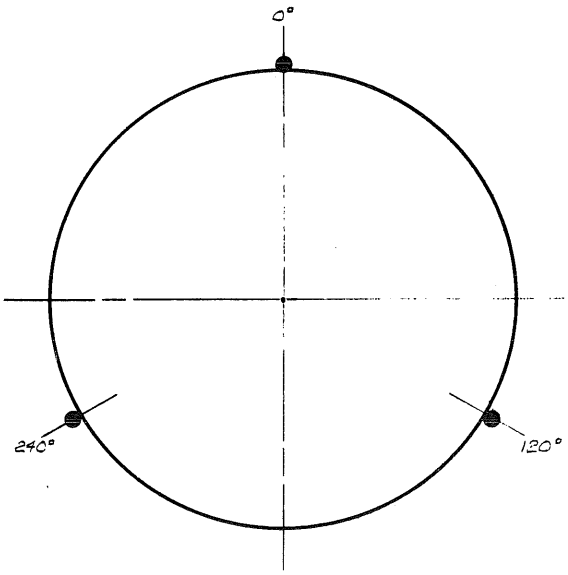

h. STATION 10s, EXHAUST NOZZLE AMBIENT, OUTER SURFACE OF NOZZLE FLAPS IN PLANE OF NOZZLE EXIT

o TOTAL PRESSURE
● STATIC PRESSURE
X THERMOCOUPLE

Fig. 6 Concluded

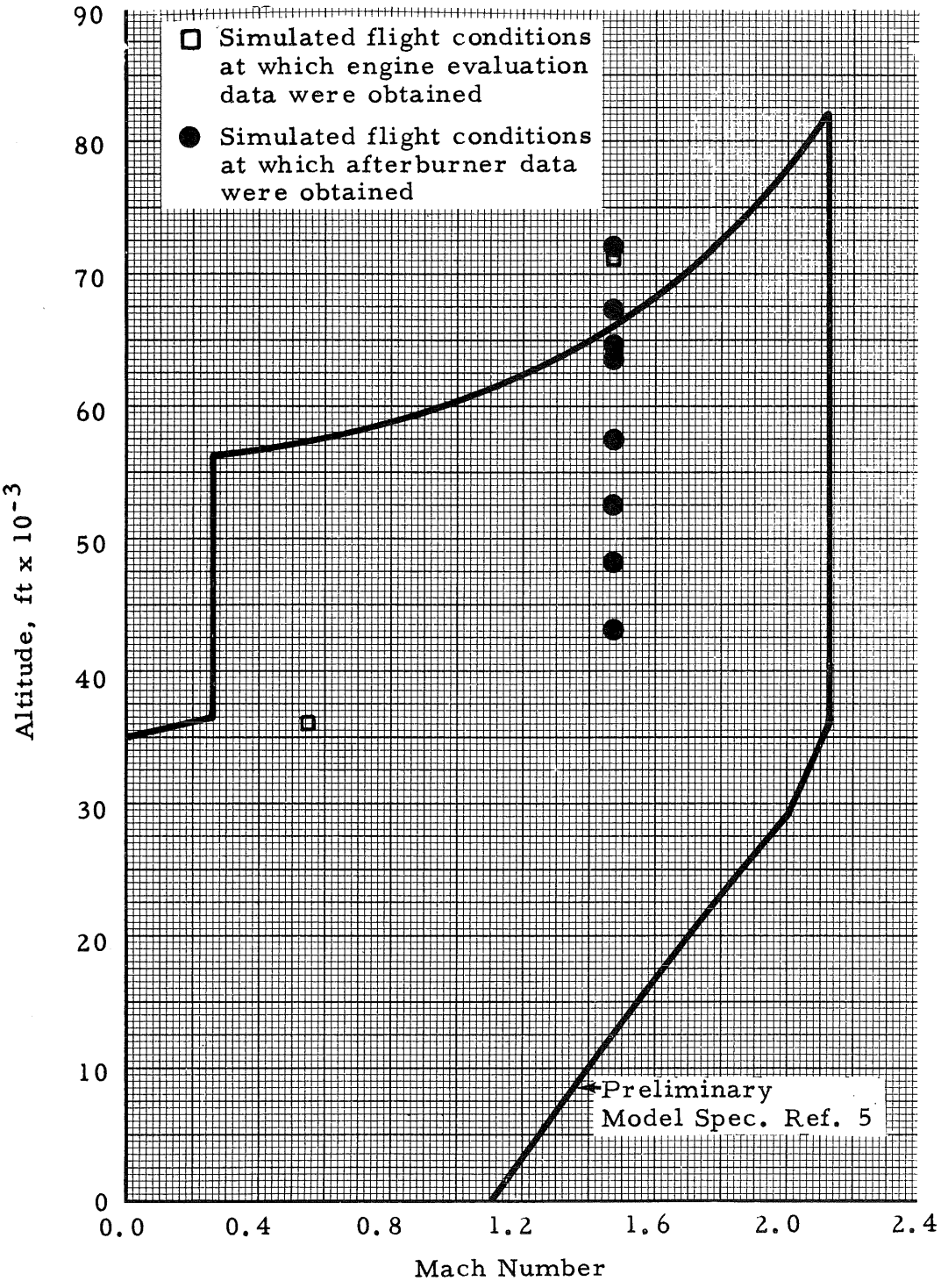

Fig. 7 Iroquois Series 2 Operational Envelope

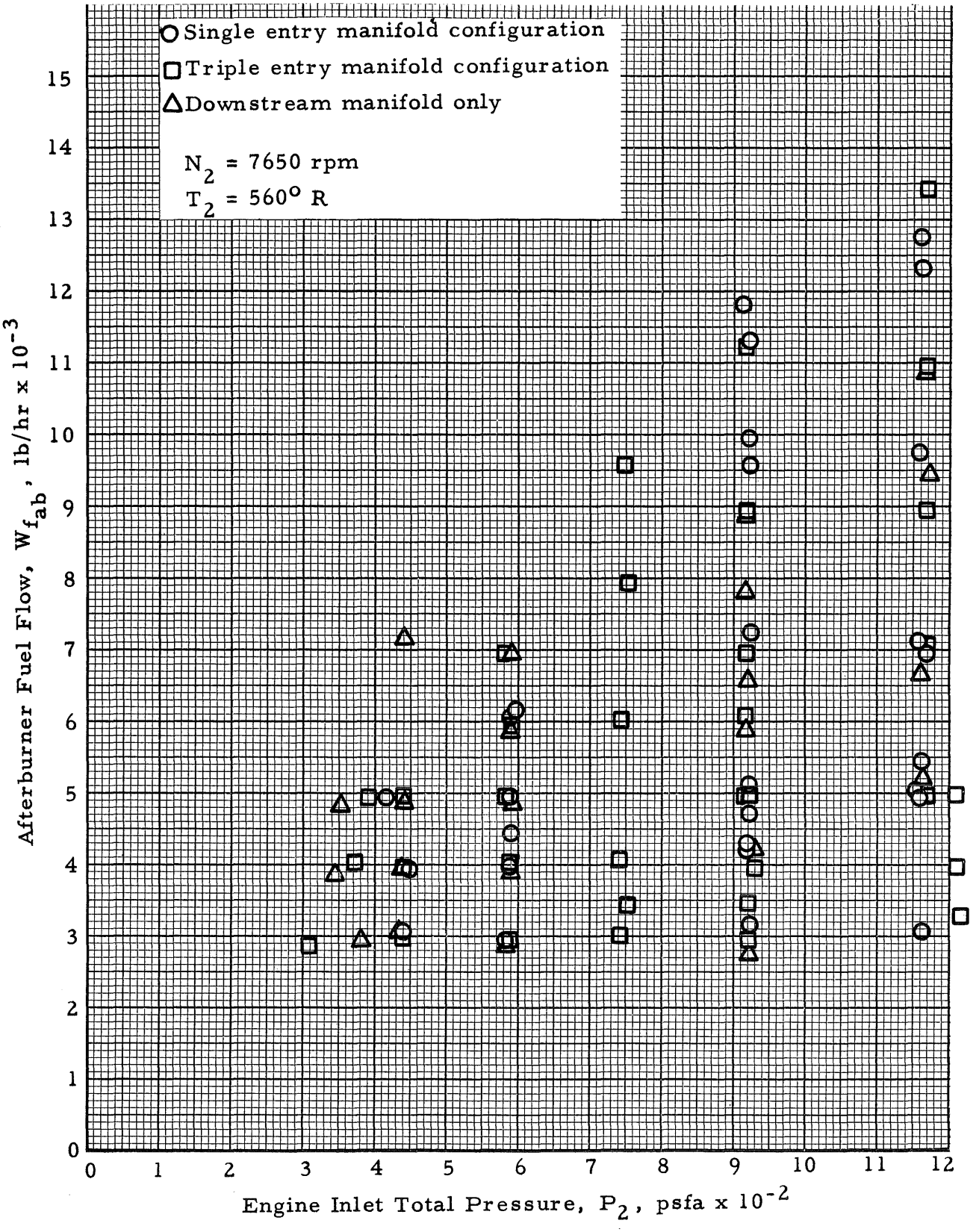

Fig. 8 Afterburner Test Data Obtained

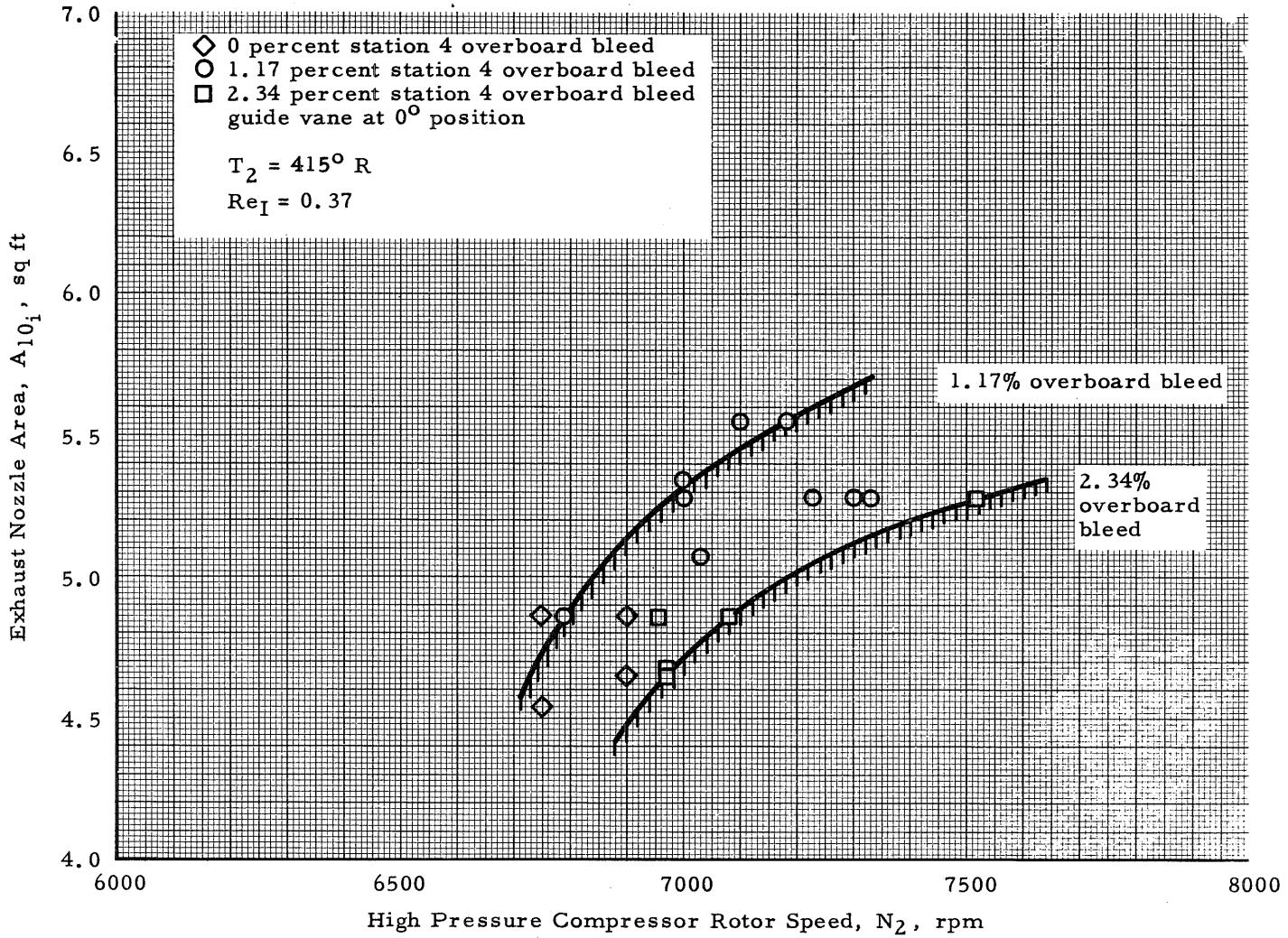

Fig. 9 High Pressure Compressor Surge Limit

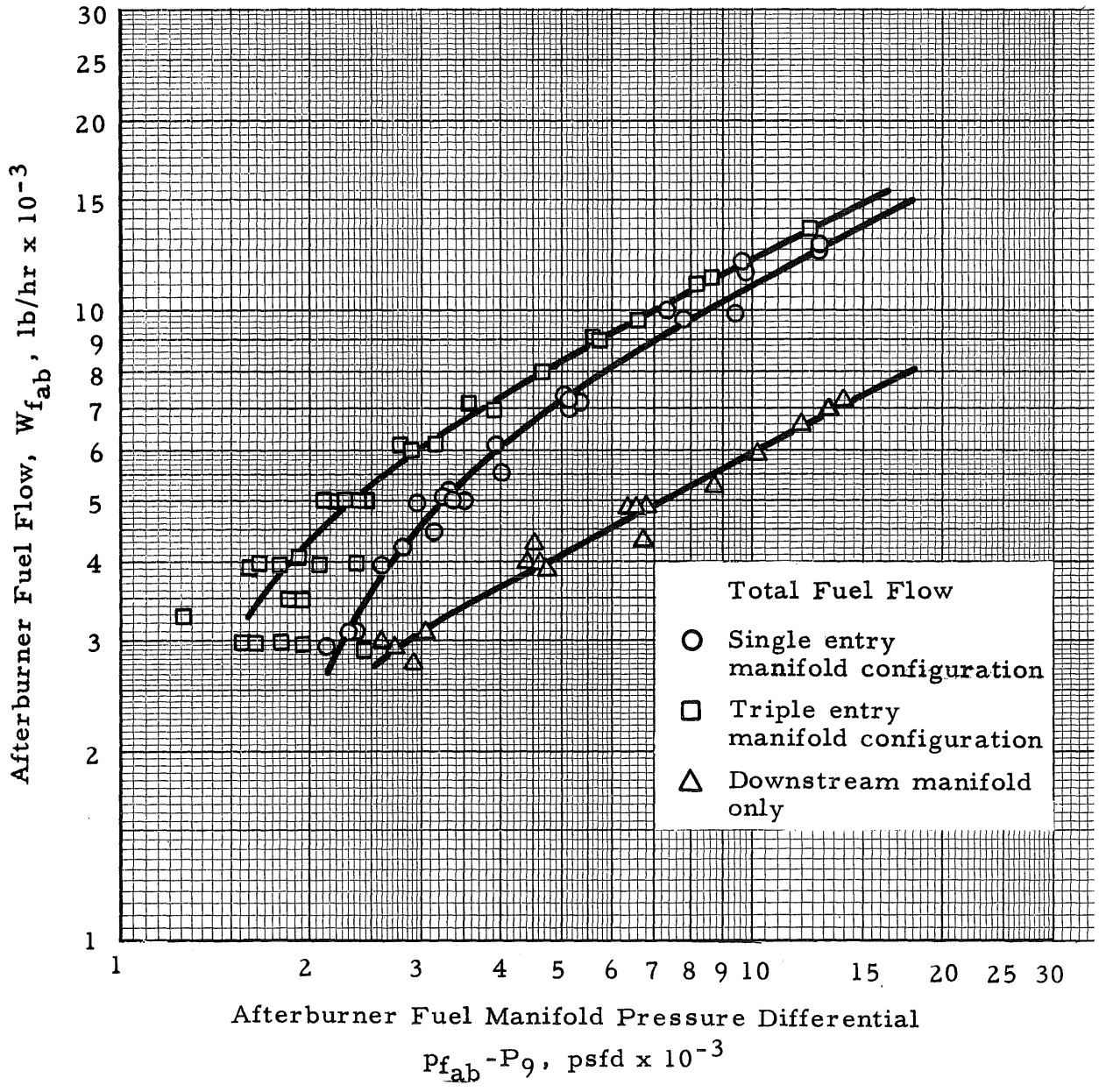

Fig. 10 Afterburner Fuel Manifold Flow Characteristics

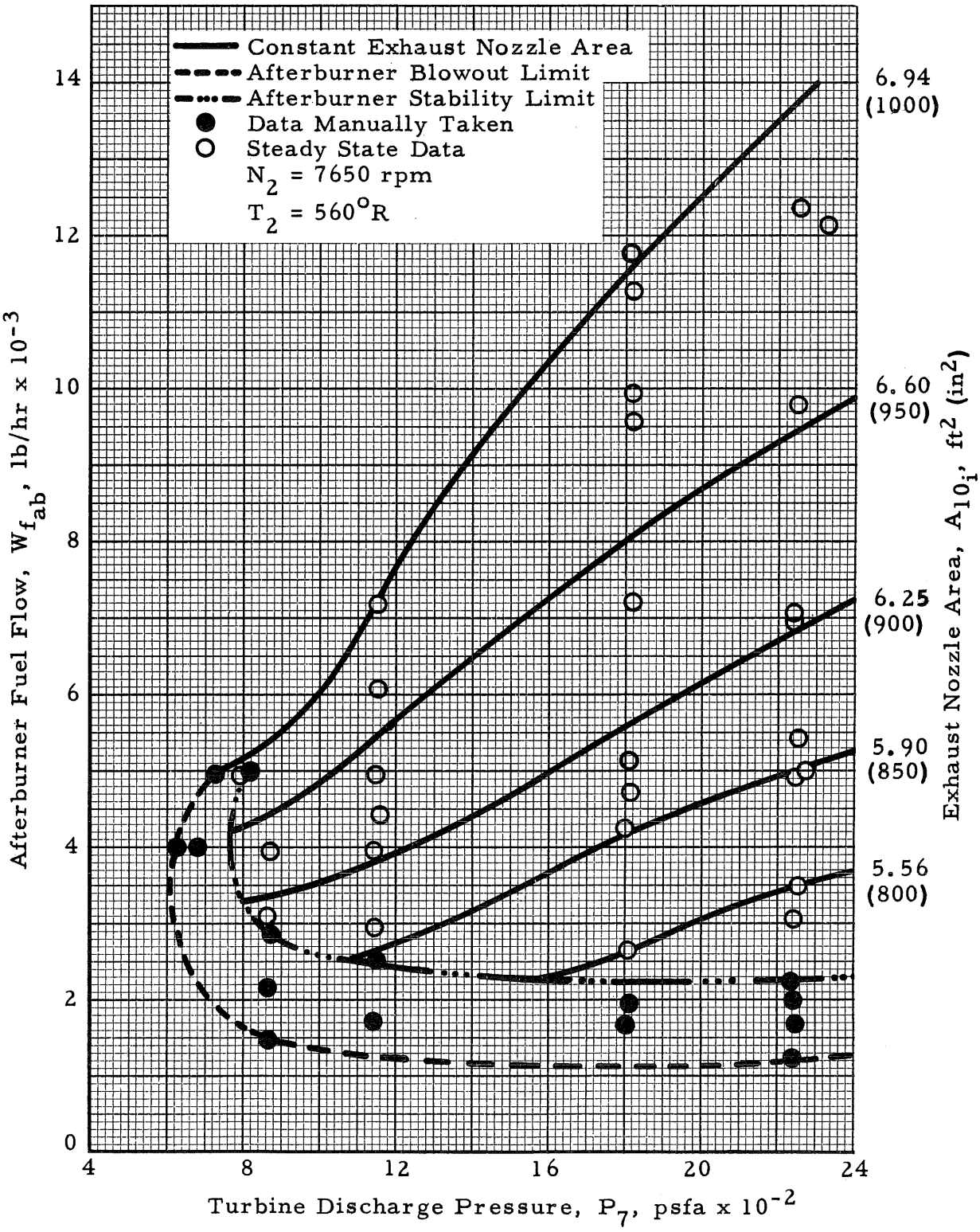

a. Single Entry Upstream Manifold Configuration

Fig. 11 Afterburner Stability Limits

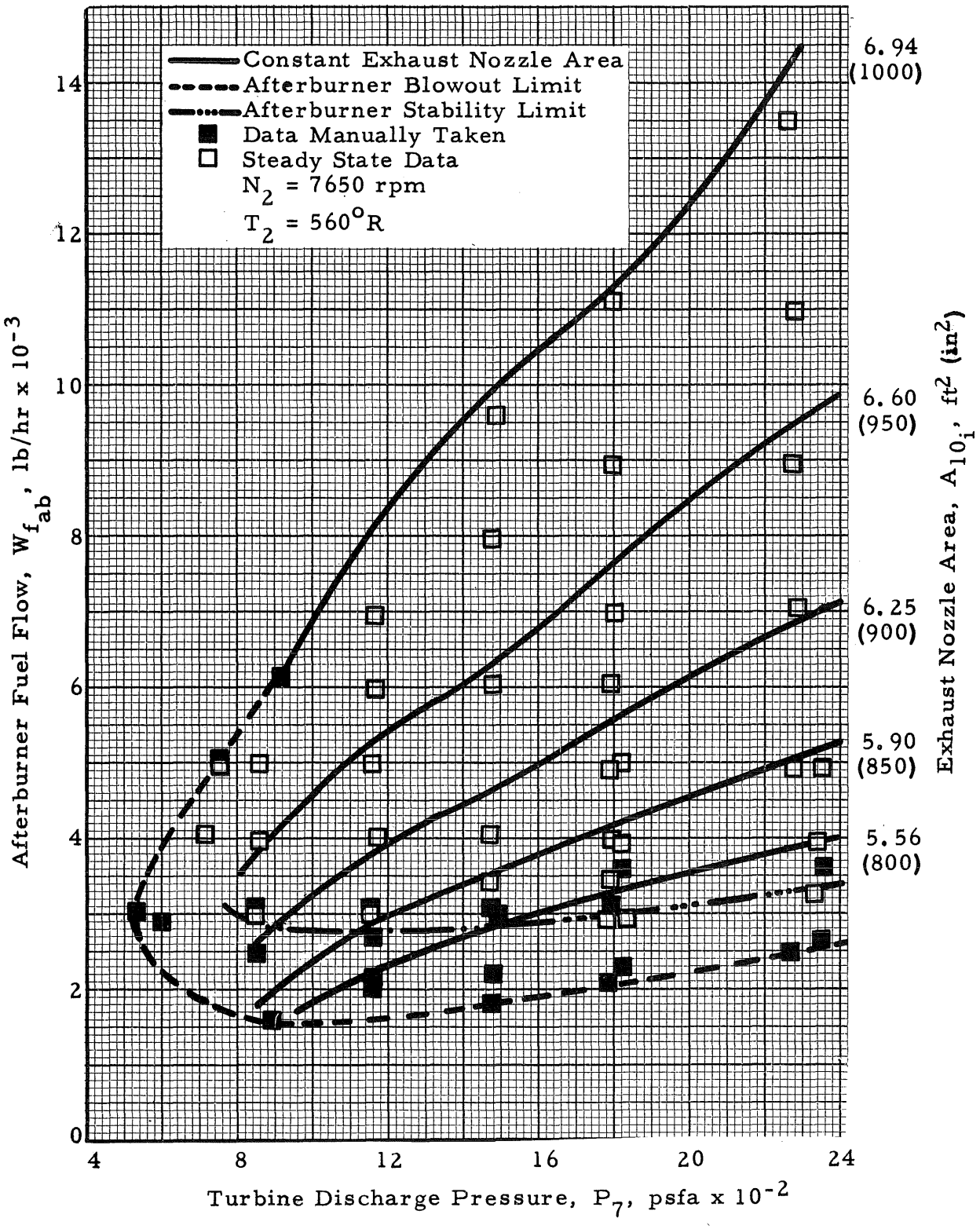

b. Triple Entry Upstream Manifold Configuration

Fig. 11 Continued

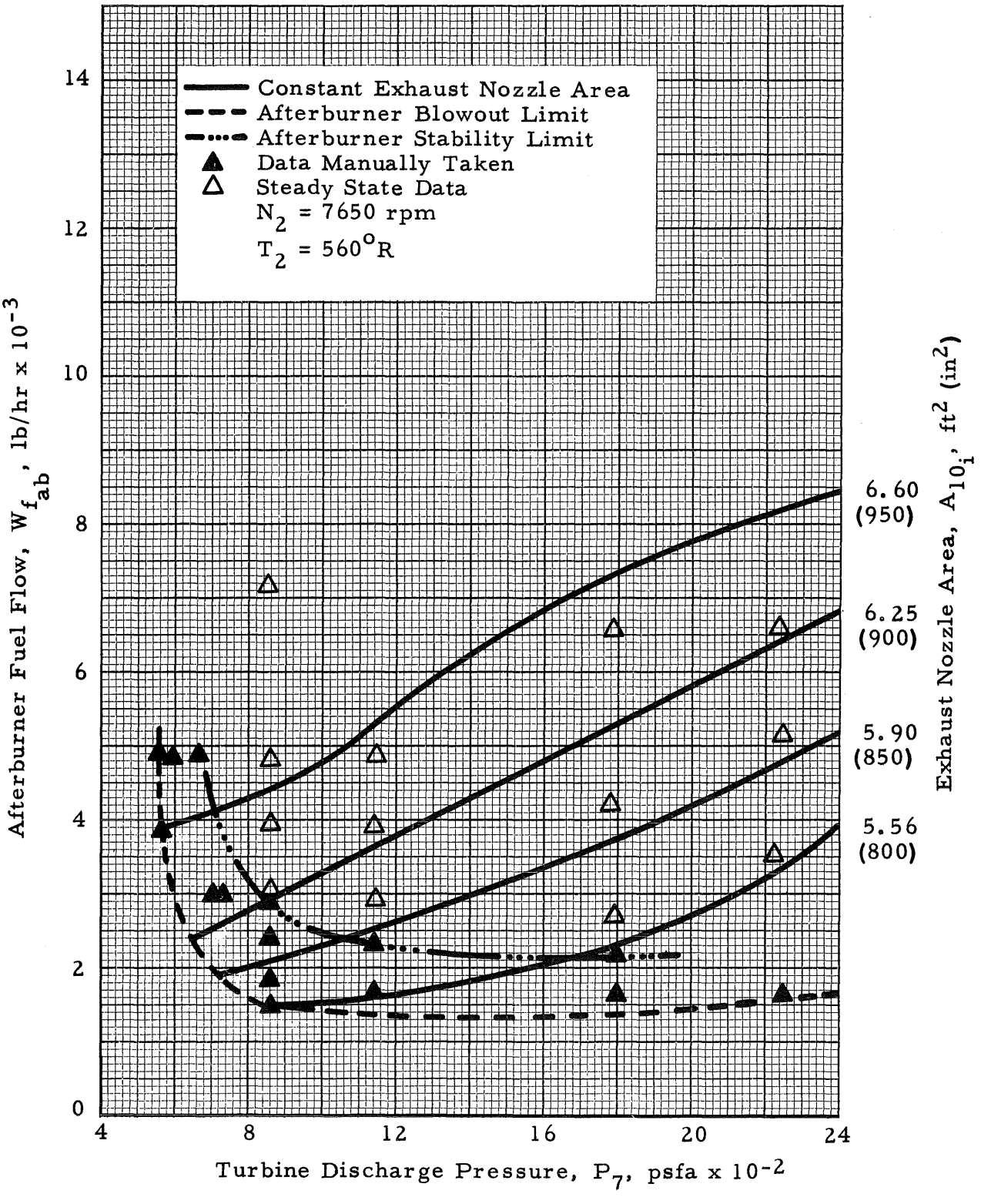

c. Downstream Manifold Only

Fig. 11 Concluded

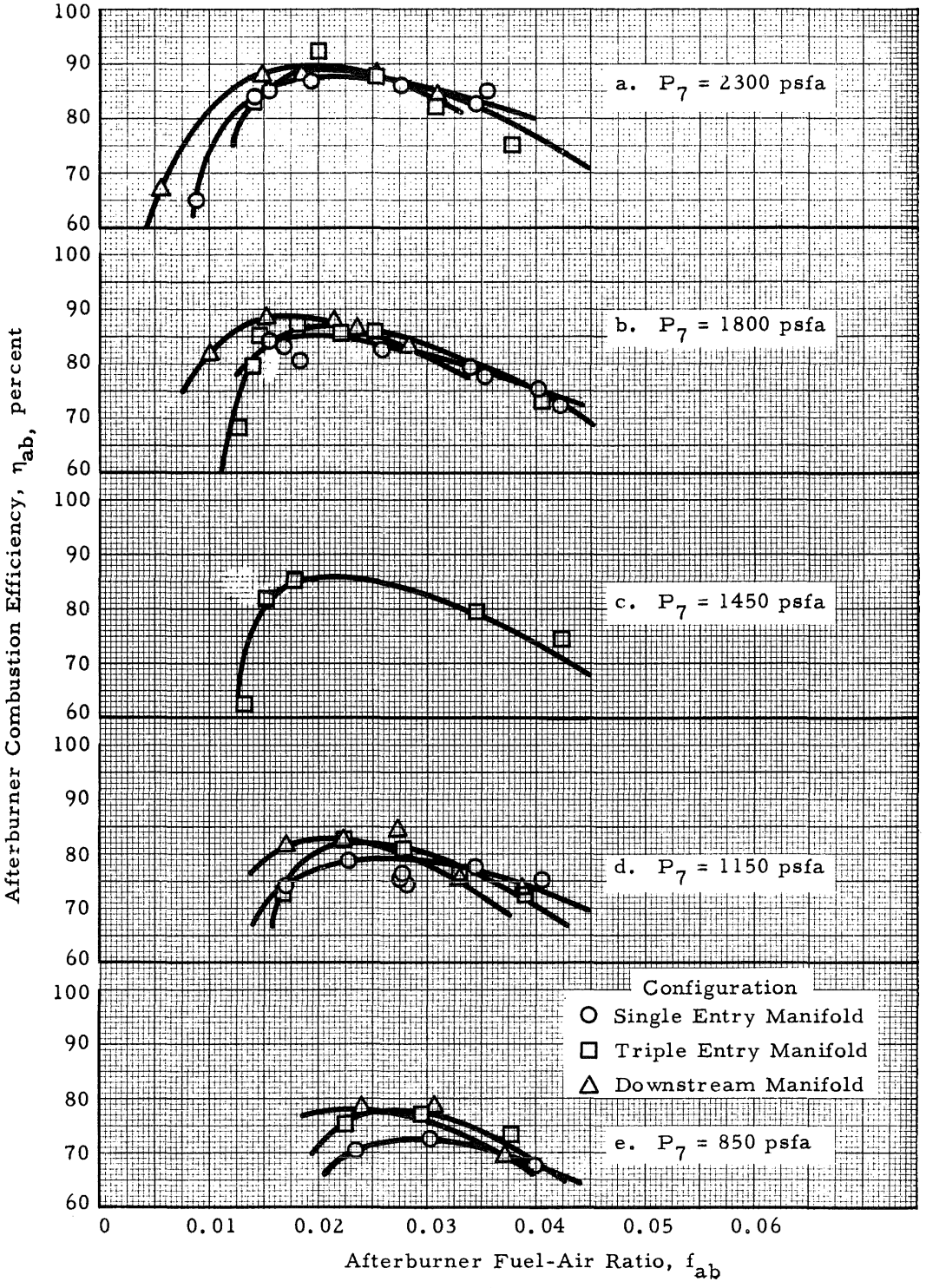

Fig. 12 Afterburner Combustion Efficiency

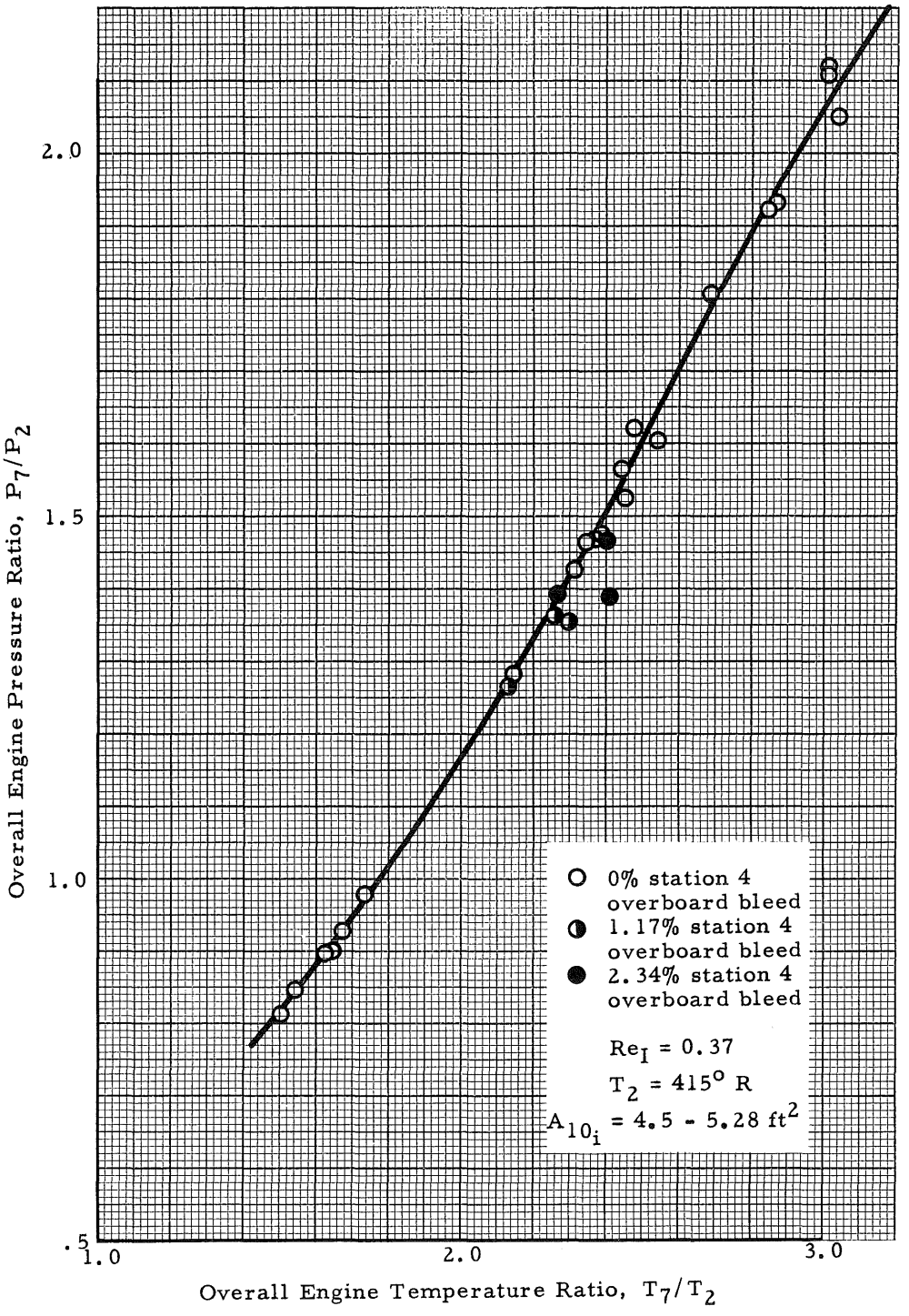

Fig. 13 Engine Pumping Characteristics

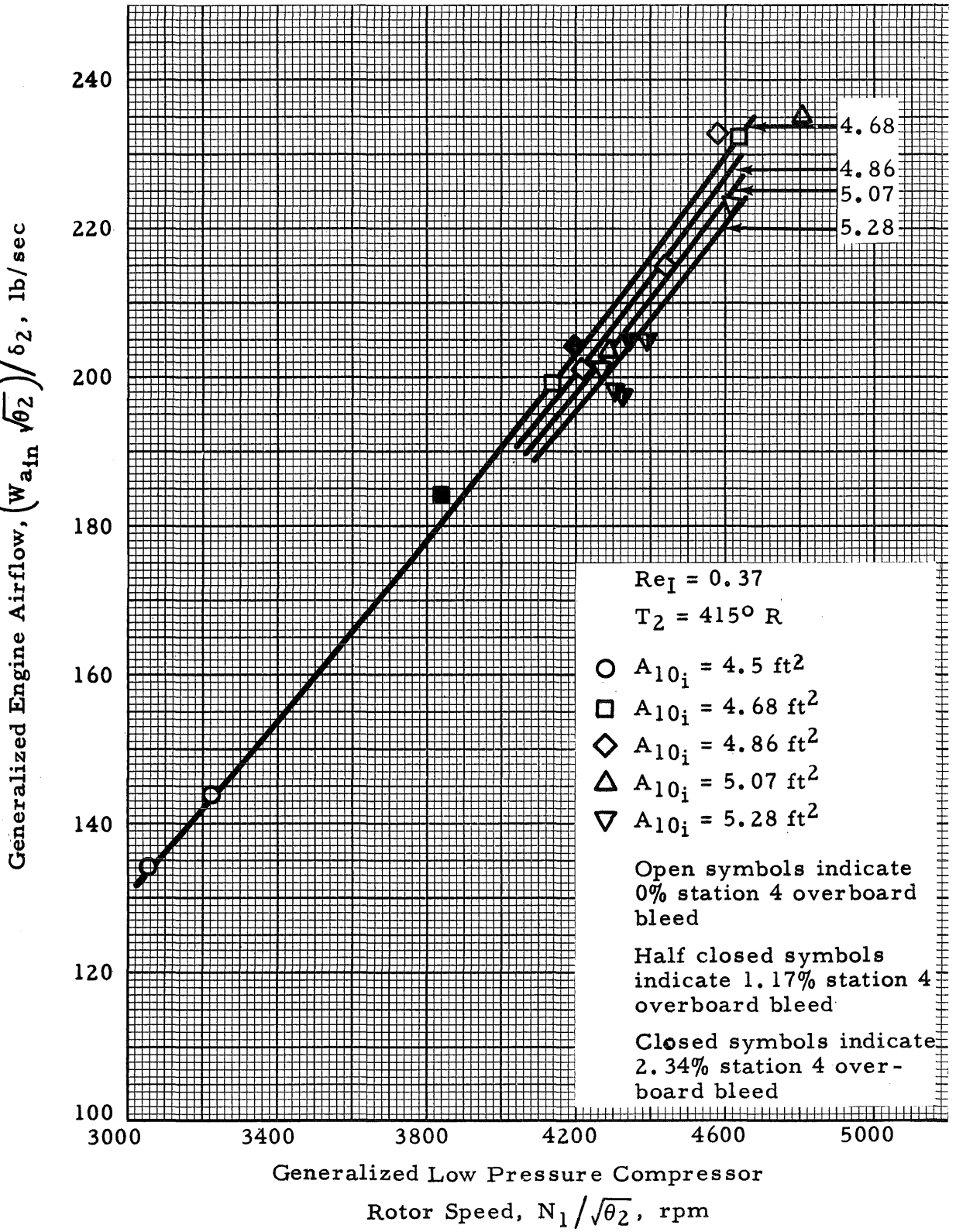

Fig. 14 Generalized Compressor Airflow

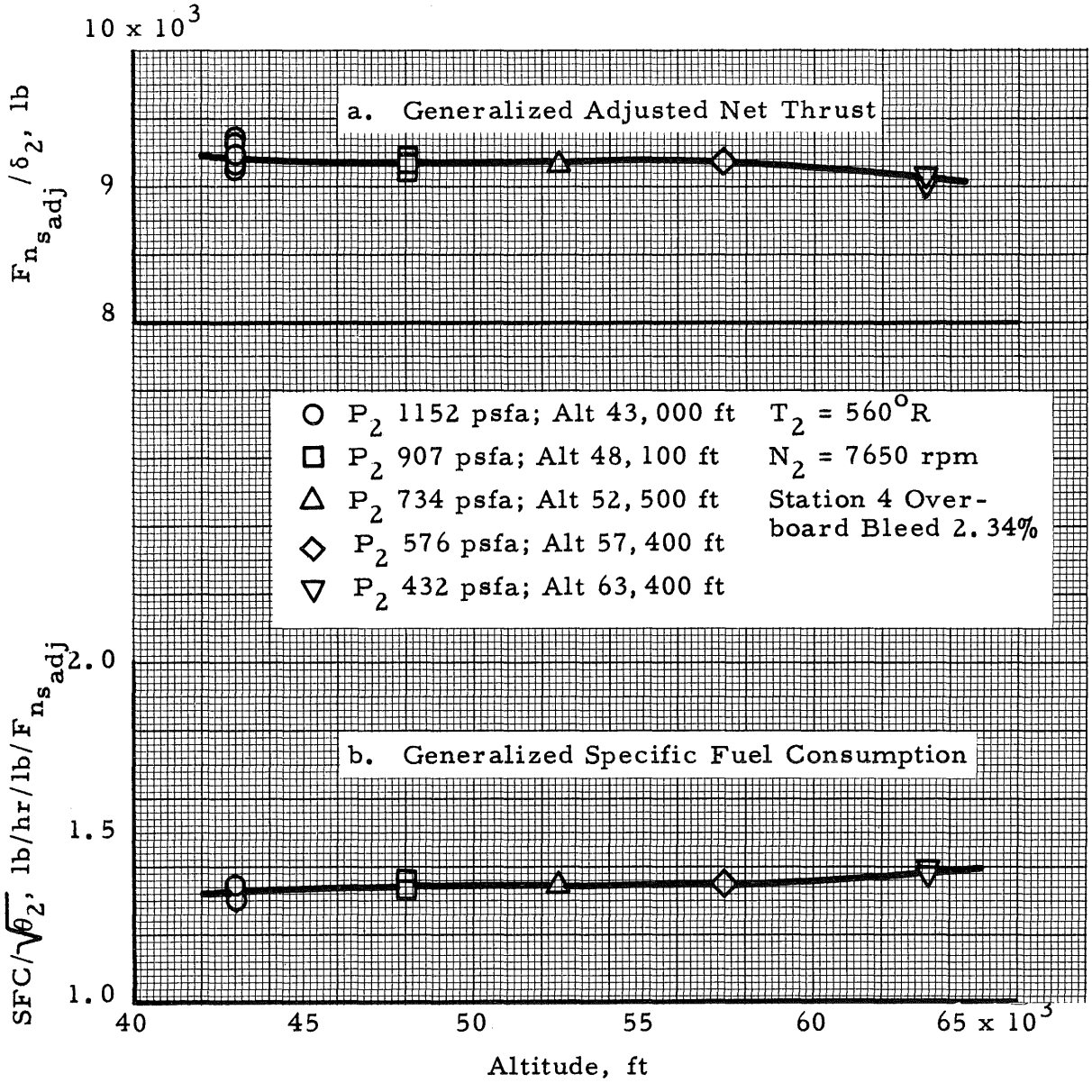

Fig. 15 Non-afterburning Engine Performance at Mach Number 1.47 at Altitude

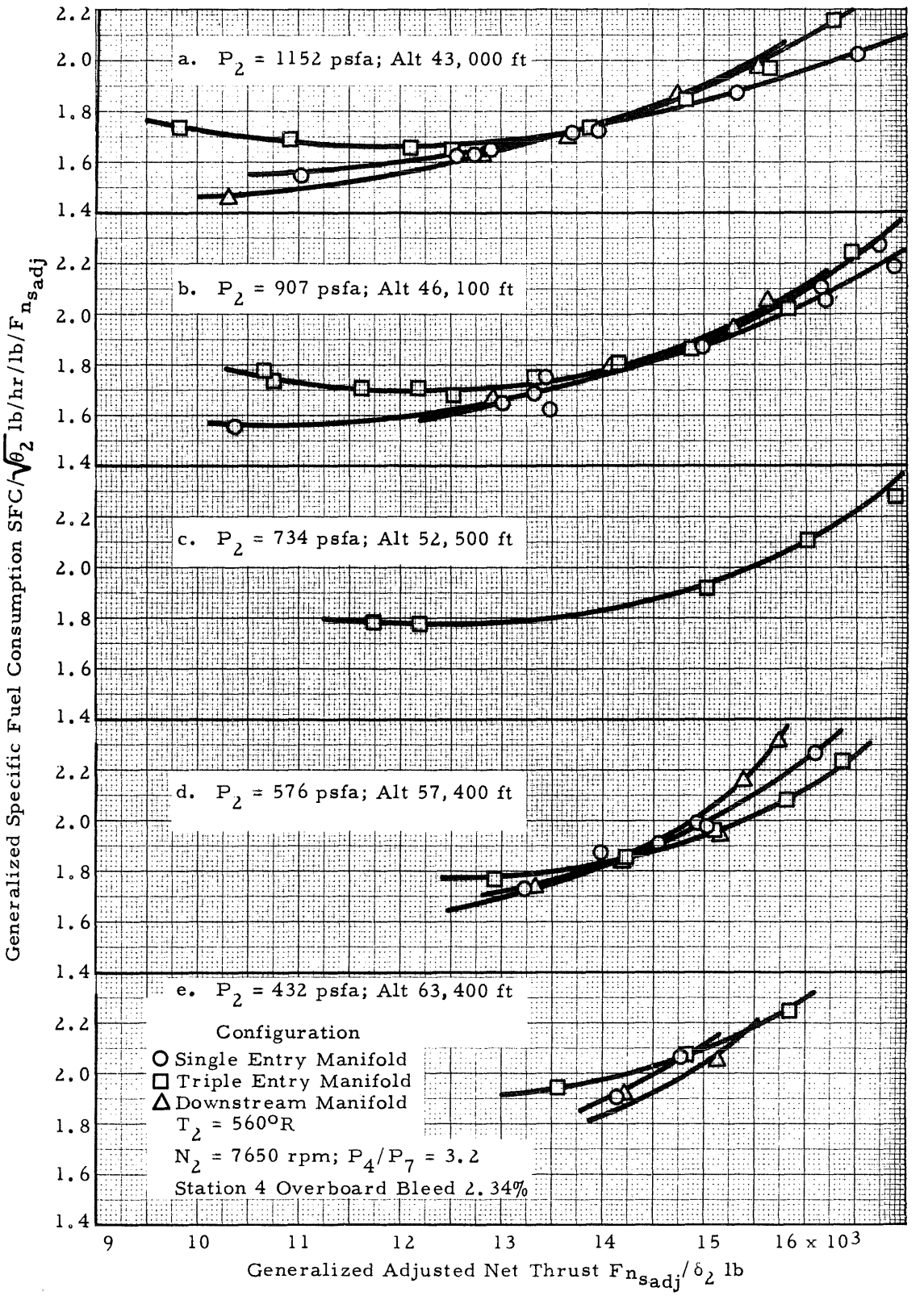

Fig. 16 Afterburning Engine Performance at Mach Number 1.47 at Altitude

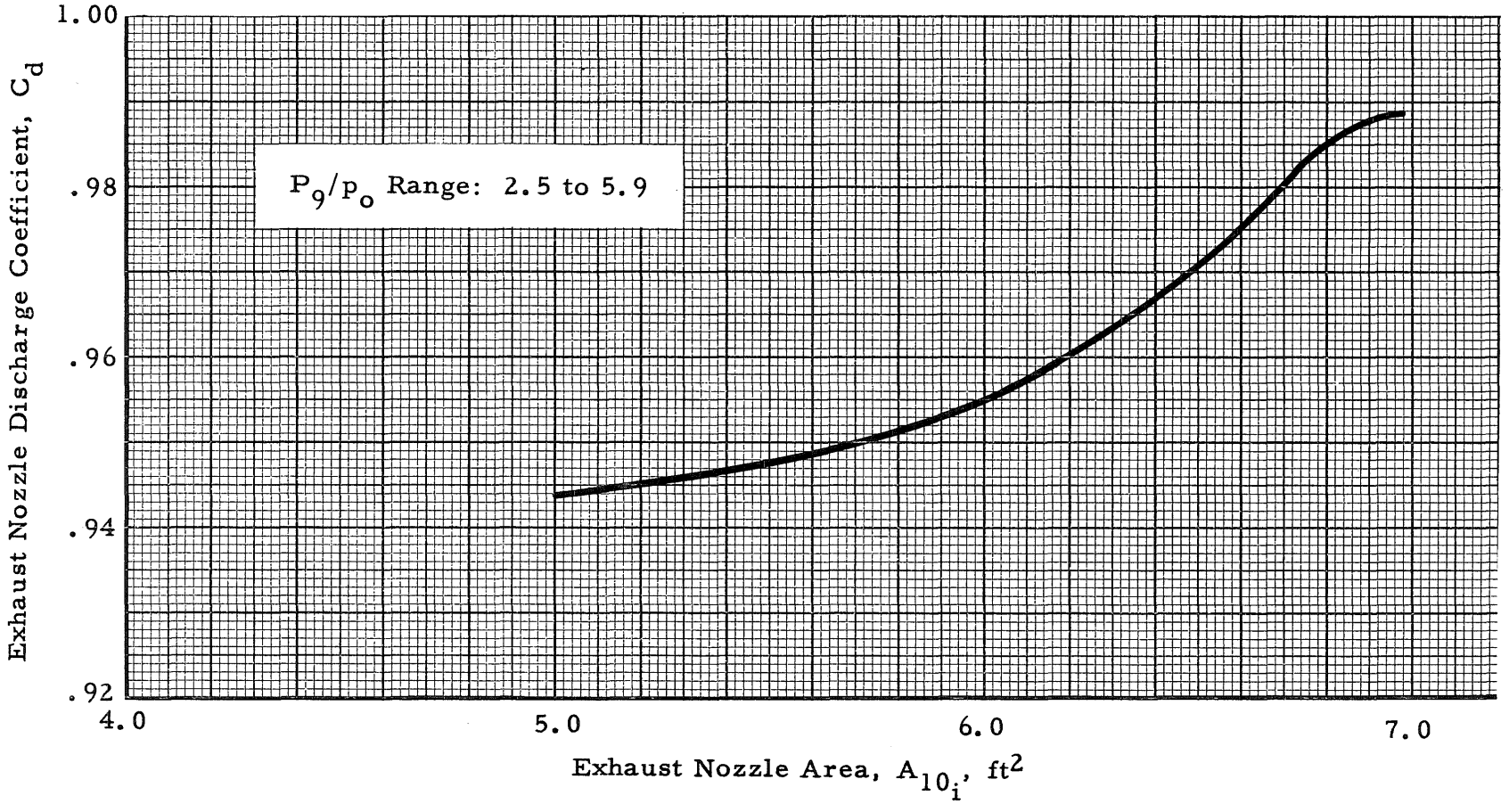

Fig. 17 Exhaust Nozzle Discharge Coefficient